# Construction of a Shielded Thermal Hall Measurement Device

by

Kaylee Biggart

A thesis
presented to the University of Waterloo
in fulfilment of the
thesis requirement for the degree of
Master of Science
in
Physics

Waterloo, Ontario, Canada, 2023

## Author's Declaration

This thesis consists of material all of which I authored or co-authored: see Statement of Contributions included in the thesis. This is a true copy of the thesis, including any required final revisions, as accepted by my examiners.

I understand that my thesis may be made electronically available to the public.

## Statement of Contributions

Our research group received 4 commercially purchased $SrTiO_3$ wafers from Michael Sutherland's group at the University of Cambridge with gold evaporated on either side of each wafer. I completed the second round of gold evaporation onto 2 of the wafers when it became necessary.

Jonathan Baugh's group at the Institute for Quantum Computing at the University of Waterloo evaporated a titanium adhesion layer and subsequent gold layer onto one $SrTiO_3$ wafer and a film of Kapton.

Data collection using Kapton-Ag wires was performed by Shaun Froude-Powers, a former undergraduate student in our research group, and I analysed the data.

I performed and analysed all sensitivity and noise resolution measurements at the University of Waterloo.

**Abstract**

A shielded thermal Hall experimental setup is being constructed and is nearing completion. An existing conventional thermal conductivity experiment was retrofit to perform thermal Hall measurements, which included the addition of coaxial cables to a low-temperature probe. A copper sample puck was machined and encases the sample, thermometers, and sample heater, to reduce mechanical stress and shield from electromagnetic radiation. $SrTiO_3$ wafers were fabricated into capacitive thermometers by evaporating gold onto either side of each wafer, and thermally resistive wires to provide electronic connection to thermometers and sample heater were fabricated by evaporating gold onto Kapton.

Preliminary testing at liquid nitrogen temperatures was performed on a sample of silver wire. Complications arose that prevented thermal conductivity or thermal Hall measurements from being performed at liquid nitrogen temperatures, but the sensitivity and temperature resolution of the capacitive thermometers was tested and found to be sufficient for detecting thermal Hall signals. It became clear that the original fabrication method used for the capacitive thermometers and Kapton wires was not robust enough to prevent the electronic components from degrading upon thermal cycling, so the use of titanium adhesion layers was explored with regards to adhering gold to $SrTiO_3$ and Kapton. Once the fabrication process for the capacitive thermometers and Kapton wires has been perfected, thermal Hall measurements can be performed using the experimental setup as described in this work.

**Acknowledgements**

First and foremost, I'd like to express my deep gratitude to my supervisor, Robert Hill. Rob's expertise and advice has been quintessential in helping me develop my experimental skills and data analysis techniques. His calm guidance has continuously helped me stay on track during times I've felt like an imposter in the lab, and has enabled me to gain confidence in myself I've never had before.

I'd also like to thank Jan Kycia for his advice on low temperature experimental techniques. Our research group has spent countless hours troubleshooting helium gas leaks in our helium recovery system, and Jan's guidance has been instrumental in our troubleshooting processes. Similarly I'd like to thank Jonathan Baugh, whose discussions around the use of a Ti adhesion layer have revolutionized our thermometer fabrication process.

I also want to thank Jennifer Reid, a former PhD student in Rob's research group. Jen and I spent many hours in the lab together, and I've learned so much about experimentalism and specifically low temperature experimentalism from her. I try to model my critical thinking and troubleshooting skills after what I observed from her in the lab. It also generally helped me build self-confidence seeing another woman in physics succeeding in her graduate studies.

Finally, I need to thank my family, without whose support I surely wouldn't be where I am. My dad Clarence has always encouraged my scientific curiosity, and always modelled the importance of hard work and attention to detail as one of the hardest working people I know. My grandparents Howard and Donna have always been there for me when I need them. They've given me the space to make mistakes, but not so much space that they couldn't pick me up when I fell down. My sister Cassie helps me blow off steam when I need to, and talks me down when I'm distressed about setbacks in the lab. Last but certainly not least, I need to thank my partner John. He has celebrated every success I've had, and he's comforted me after every failure. His love and support has enabled me to focus solely on finishing my MSc project, and I don't know where I'd be without him.

## Dedication

*For John and Toven.*

# Contents

# List of Figures

# List of Tables

# Chapter 1

# Introduction

Every piece of technology that we have come to use, depend on, and perhaps even loath, is available to us for one reason — humans are curious, and we do not stop poking our discoveries with a metaphorical stick. For example, Alexander Graham Bell invented the telephone, and now we have cell phones that, while still capable of making phone calls, are now largely used for scrolling social media or browsing an online library of millions of videos — something Bell could never have imagined. That is an example of the global strategy used to further advancements in material science: a discovery is made, a new material is synthesized, properties of that material are measured, leading to a new discovery being made, and so forth. Our research group is able to utilize new measurement techniques to break ground on the study of exotic physical phenomena, and thus play a crucial role in this global strategy.

The investigation of transport properties of a material is an important piece of this global strategy. Thermal transport properties in particular can be useful in understanding delocalized excitations of a material — studying the way a material responds to an applied temperature gradient provides information on the types of mobile entropy carriers exist in the material and thus can be used to characterize the behaviour of the material. One particularly intriguing area of interest in studying thermal transport properties is to perform thermal Hall measurements on materials of interest. The thermal Hall effect can be thought of as a thermal analog to the conventional Hall effect, can be used to study exotic and novel behaviours by investigating a transverse temperature gradient produced in a material when a magnetic field is applied perpendicular to an applied longitudinal temperature gradient.

Construction of a thermal Hall experimental setup is nearing completion.

Complications around fabrication of thermometers used in the setup have been investigated and, once resolved, the experimental setup will be ready to perform experiments on materials with complex behaviours, such as proposed topological Kondo insulator $SmB_6$. This thesis details the construction and testing process, from describing what the thermal Hall effect is and why it can be used to study novel physical phenomena, to the current state of the setup and the next immediate steps that will be taken to complete construction. The thesis is thus separated into two parts. Part I consists of two chapters — chapter 2 describes what the thermal Hall effect is, how it *can* be used to study complex materials, and how it *has* been used to study such materials. Chapter 3 then discusses a proposed material of interest that will be studied using the experimental setup of this work.

Part II describes the experimental setup and results of preliminary testing of the setup. Chapter 4 describes the setup in detail, and explains why specific design choices were made. Chapter 5 describes the results of a first round of testing of the setup, as well as the discovery that there was a flaw in the fabrication of the thermometers used. Chapter 6 discusses a new fabrication technique for the thermometers as well as preliminary testing results after having employed this new technique. Finally, chapter 7 discusses the next immediate steps that will be taken to complete construction of the setup.

# Part I

# Theory

# Chapter 2

# Thermal Hall Effect Background

## 2.1 Thermal Conductivity Background

A thermal current can be thought of as the heat analogue of an electronic current —entropy carriers move to produce a thermal current, just as charge carriers move to produce an electronic current. However, the mechanism behind each phenomenon is quite different. To produce an electronic current, charge carriers move in response to an applied electrical potential difference. A thermal current on the other hand is produced when entropy carriers (which can be charged or charge-neutral) are subject to a temperature gradient.

Thermal conductivity is a measure of how readily heat flows through a particular material. In other words, thermal conductivity is to a heat current what electronic conductivity is to an electronic current. The thermal conductivity of a material may be computed from Fourier's law of heat conduction:

$$\vec{J}_i = -\kappa_{ij}\vec{\nabla}T_j \tag{1}$$

Where $\vec{J}_i$ is the heat flux per unit area in direction $i$, $\kappa_{ij}$ is the thermal conductivity tensor, and $\vec{\nabla}T_j$ is the temperature gradient in direction $j$.

Generally speaking, $\kappa_{ij}$ is a 2nd rank tensor which allows for not only directional anisotropy depending on the axis that a temperature gradient is applied, but also allows for heat currents transverse to the axis of the applied temperature gradient. Equation 1 may be simplified by focusing on heat conduction in a particular dimension, and simplifies to:

$$\dot{Q} = -\kappa\Delta T\frac{A}{L} \tag{2}$$

Where now $\dot{Q}$ is the heat power supplied to a sample in a specified direction, $\kappa$ is now a scalar quantity representing the thermal conductivity the direction specified by $\dot{Q}$ is applied, $\Delta T$ is the temperature gradient in the direction specified by $\dot{Q}$, $A$ is the cross-sectional area of the thermal current flow perpendicular to the temperature gradient, and $L$ is the length of the sample along which the temperature gradient is measured.

Since thermal conductivity measurements are a measure of how entropy carriers move through a material, thermal conductivity measurements are a probe of the bulk [1]. For example, thermal conductivity measurements have been used to characterize magnetic excitations in classical spin ice materials $Ho_2Ti_2O_7$ (HTO) and $Dy_2Ti_2O_7$ (DTO), and quantum spin ice material $Yb_2Ti_2O_7$ (YbTO) [2]. Thermal conductivity measurements have also been used to characterise the symmetries of unconventional superconductor $Nd_2CuO_4$ by studying the phonon contribution to thermal conductivity at low temperatures compared with electronic quasiparticle excitations [3].

## 2.2 The Thermal Hall Effect

A second rank tensor, $\kappa_{ij}$ in equ. 1 can in principle be anisotropic. This means that $\kappa_{ij}$ is not necessarily equivalent to $\kappa_{jk}$, $\kappa_{ki}$, $\kappa_{ji}$, etc. It also means that, if a temperature gradient is applied in one direction, a heat current may be observed in another direction, under certain conditions.

In certain materials, if a longitudinal temperature gradient is applied, and the sample is placed in a magnetic field perpendicular to the $ij$ plane, a transverse heat current may be observed. This phenomenon is called the thermal Hall effect. It can be thought of as the thermal analogue of the electrical Hall effect, where a transverse electrical current is observed due to the Lorentz force acting on charge carriers arising from the presence of the magnetic field.

An important distinction however is that a Lorentz force isn't necessarily the only cause for a transverse thermal current. For example, charge neutral excitations such as magnetic excitations [4] and phonons [5] have been observed to contribute to a transverse thermal current, neither of which would be subject to a Lorentz force. In other words, the thermal Hall effect can be employed as a probe of novel and exotic physical phenomena.

## 2.3 Examples of Thermal Hall Applications in Exploring Novel Excitations

### 2.3.1 Phonon Hall Effect

In one example of the thermal Hall effect being used to probe bulk charge neutral excitations, Grissonnache *et al.* [6], [5] performed thermal Hall measurements on the cuprate superconductors $La_{1.6-x}Nd_{0.4}Sr_xCuO_4$ and $La_{1.8-x}Eu_{0.2}Sr_xCuO_4$. In the regime where the samples are in a pseudogap phase, a large transverse thermal conductivity was observed, as seen in figure 2.1a. This response was not observed outside of the pseudogap phase. Additionally, the magnitude of this thermal Hall response was approximately the same in the xy and yz directions (see fig. 2.1b). This translates to an approximately equal thermal Hall response both parallel and perpendicular to copper oxide planes, and the only entropy carriers that can move along and through such planes are phonons [5]. From this, they were able to conclude that phonons were the source of the transverse thermal current.

This was a surprising result, as phonons are spinless, they would not experience a Lorentz force. In fact, Grissonnanche *et al.* at first dismissed the idea that phonons were causing such a large thermal Hall current [6]. It appears as though the phonons are coupling to some intrinsic property of the system (ie., an electronic degree of freedom) rather than some extrinsic property (ie., impurities). The idea of phonons scattering from sample impurities in particular was dismissed, because there was no thermal Hall signal observed for doping levels above the critical doping $p*$, where the sample experiences no pseudogap phase. All samples had the same level of impurities, so if phonons were scattering off of impurities, all samples should have seen the same thermal Hall response. In other words, thermal Hall measurements of $La_{1.6-x}Nd_{0.4}Sr_xCuO_4$ and $La_{1.8-x}Eu_{0.2}Sr_xCuO_4$ showed that, in the pseudogap phase, phonons are coupling to some intrinsic property of the system and gaining chirality, though at this time this phenomenon is not fully understood.

### 2.3.2 Circulating Majorana Fermions

Thermal Hall measurements can also be useful in probing topological states. For example, measurements were performed on $\alpha - RuCl_3$ [7], [8]. The sample was placed in a magnetic field parallel to the c-axis of the sample (see fig. 2.2), and a heat current was applied parallel to the a-axis.

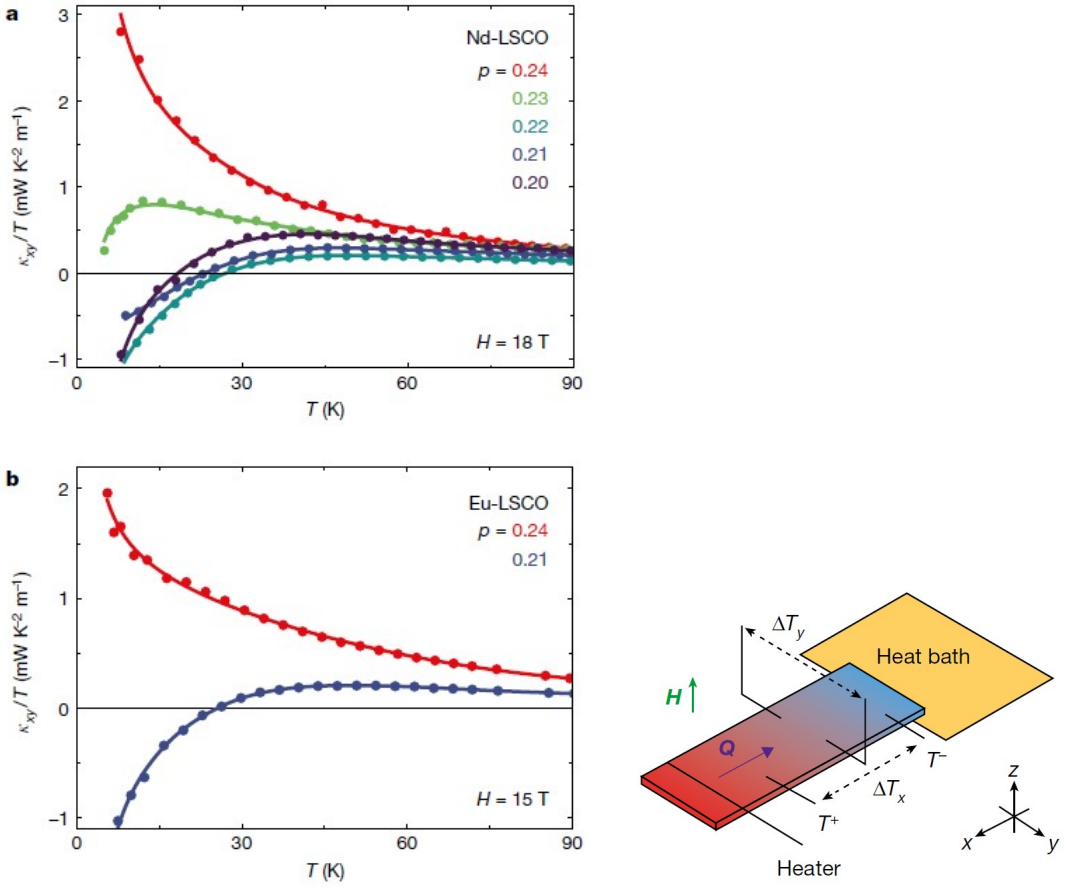


(a) Data (b) Schematic

Figure 2.1: Experimental setup and data from [6]. a) Data: Thermal Hall response from [6] of $La_{1.6-x}Nd_{0.4}Sr_xCuO_4$ (**a**) and $La_{1.8-x}Eu_{0.2}Sr_xCuO_4$ (**b**). In both cases, the critical doping level is $p* = 0.23$. It can be seen that the thermal Hall response becomes negative at low temperatures only for $p < p*$ — inside of the pseudogap phase. b) Schematic: Schematic of experimental setup from [6]

In this study, Kasahara *et al.* [8] observed that the thermal Hall signal was half-integer quantized, with quantum units of $\frac{\pi}{6}\frac{k_B^2}{\hbar}\frac{1}{T}$ (seen in figure 2.3), which is consistent with that of a Kitaev spin liquid [7], [8]. It was proposed that the applied field forces the sample into a Kitaev spin liquid state and in this state, Majorana fermions circulate around the edges of the sample and carry heat (see figure 2.4), causing a transverse temperature gradient to appear.

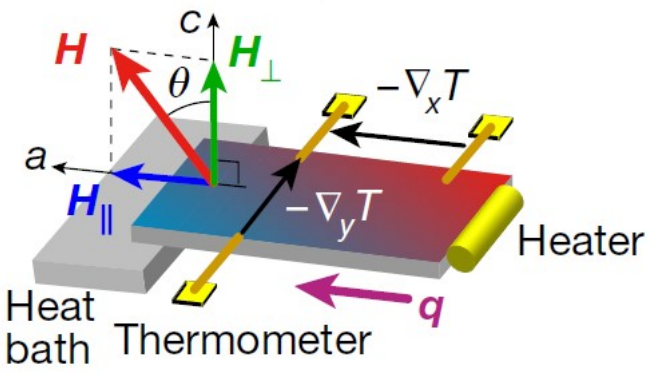


Figure 2.2: Schematic of experimental setup from [8]

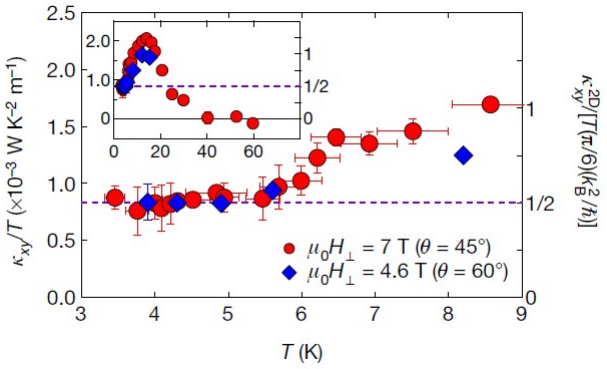


Figure 2.3: Temperature dependence of $\kappa_{xy}/T$ from [8]. The main panel shows the low temperature behaviour while the inset shows the temperature dependence for the entire range of data.

By probing the thermal Hall effect of the sample in the proposed Kitaev spin liquid state, one is effectively probing the circulation of Majorana fermions. That is to say, by probing a bulk property (thermal Hall current), one is able to directly probe the band topology, as the existence of circulating Majorana fermions has been interpreted as an implication of a Kitaev spin liquid [7], [8].

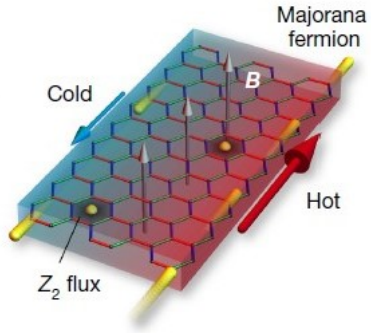


Figure 2.4: Schematic of heat conduction due to circulating Majorana fermions [8]. The red (blue) arrow represents the movement of hot (cold) Majorana fermions (yellow balls), the grey arrows represent the direction of the applied magnetic field (which is variable, see figure 2.2). A temperature gradient is applied parallel to the red arrow, and since the Majorana fermions are circulating counter clockwise around the sample, a transverse temperature gradient is produced.

### 2.3.3 Concluding Remarks

Sections 2.3.1 and 2.3.2 demonstrate that thermal Hall measurements can be wielded as a powerful probe of complex and often strongly correlated systems. With this idea in mind, chapter 3 outlines a proposal for studying the behaviour of the complex and strongly correlated topological Kondo insulators using the thermal Hall effect.

# Chapter 3

# Proposal: Using the Thermal Hall Effect to Study Topological Kondo Insulators

Topological Kondo Insulators (TKI's) are materials that have an electrically insulating bulk and electrically conducting surface [9], and are complex, strongly correlated systems subject to exotic physical phenomena. Being a probe of exotic bulk phenomena, thermal Hall measurements provide an intriguing opportunity to further understand TKI's. In order to understand TKI's, it's necessary to first understand topological insulators (TI's) and Kondo insulators (KI's). The contents of this chapter are just a brief summary of rather complex and interconnected concepts — Franz and Molenkamp dedicate an entire textbook to the topic of topological insulators [10] and Coleman dedicates 3 chapters of [11] to the Kondo effect and TKI's. This overview of TKI's and $SmB_6$ motivates the need for a thermal Hall experimental setup to be constructed, as thermal Hall measurements may be instrumental in uncovering the exotic and hotly debated behaviours of $SmB_6$.

## 3.1 Topological Insulators

A conventional insulator is a system whose Hamiltonian can be adiabatically transformed to a model with all electrons bound to an atom in closed shells, without inducing any phase transitions [12] (similarly, the state of an atomic insulator can be adiabatically transformed to a vacuum state). There are, however, insulators that have a "twist" to their electronic wave function that prevents their Hamiltonian from being adiabatically transformed into

an atomic insulator, and these materials are called Topological Insulators (TI's) [9].

The result is an insulating bulk that cannot be adiabatically transformed into a trivial atomic insulator. In other words, there exists a boundary between the insulating bulk and vacuum, and the band gap in the bulk is required to close at this boundary — the surface [13]. This causes conducting surface states to arise. Typically surface states are sensitive to disorder, and surface reconstruction will cause surface states to dissipate [9]. However, in a topological insulator, these surface states are topologically protected and are therefore long-lived [12]. This is due to the "twist" in the material's wave function, which may originate from spin orbit coupling of $f$ shell electrons, driving band inversion, opening a band gap in the bulk [9].

## 3.2 The Kondo Effect and Kondo Insulators

It has been observed that in some materials, as temperature is decreased, resistance decreases, reaches a minimum at a characteristic temperature (called the Kondo temperature $T_K$), and starts to increase again. This resistance minimum was found to be caused by magnetic impurities in the materials [14]. The Kondo effect can be observed in materials containing specifically a magnetic impurity. The local moment of the magnetic impurity causes a local magnetic moment, which interacts with conduction electrons [11].

Above $T_K$, the local moment is emersed in a Fermi sea [15]. The local moment maintains a spin degree of freedom, and conduction electrons scatter off of the local moment as described by perturbative scattering theory [14]. Below $T_K$, instead of magnetic order developing, the magnetic moment of the impurity is screened by the Fermi sea [15]. Conduction electrons scatter off of the impurity, causing an increase in resistance with a decrease in temperature [14]. Since the spin of the magnetic impurity is coupled to the momentum of the conduction electrons, if the spin is flipped by an electron scattering off of the impurity, so is the momentum of the electron. Thus the resistance of the material increases with decreasing temperature, rather than plateauing.

A Kondo insulator (KI) is a material that has a lattice of localized $f$ electrons emersed in a sea of conduction electrons. Each lattice site can then be viewed as a localized magnetic moment — ie., the material has a lattice of Kondo moments interacting with conduction electrons. Above $T_K$, the mag-

netic moments remain localized and conduction electrons simply scatter off of them but below $T_K$, spin orbit coupling dominates [9]. This causes band hybridization between the conduction and $f$ shell electrons. Band hybridization opens a band gap and, if the Fermi level of the material falls in this gap, the material becomes insulating, with the energy of the gap dictating the temperature scale of $T_K$ [11].

## 3.3 Topological Kondo Insulators

In 2010 it was proposed that KI's may be trivial or non-trivial insulators which, in the context of TI's means that non-trivial KI's may host topologically protected surface states [16]. As outlined in section 3.2, in a KI, $f$ electrons hybridize with conduction electrons to open a band gap, which has an energy scale on the order of 10 meV [9]. Spin orbit coupling of $f$ shell electrons in a KI has a larger energy scale of 0.5 eV, which Dzero *et al.* calls "essentially infinite spin-orbit coupling" [9] — because the spin orbit coupling energy scale is so large compared with the KI's band gap energy scale, it can introduce topologically protected conduction surface states.

Additionally, as discussed in section 3.2, in a KI the $f$ electron bands hybridize with the conduction bands. When the $f$ electrons experience spin-orbit coupling, degeneracies are lifted, and the $f$ electrons are no longer dispersionless. These dispersive $f$ electrons, which typically have odd parity, hybridize with conduction electrons, which typically have even parity. This means that, when the bands hybridize and renormalize, the bands cross each other causing band inversion. If this occurs an odd number of times, it results in a weak topologically insulating state. [9]. This is in contrast to a model for a conventional Kondo insulator, where band topologies are not considered, and the hybridized bands instead both have the same parity, as seen in figure 3.1. Spin orbit coupling contributions, and therefore topological properties, are encoded in the hybridization matrix [9].

## 3.4 Topological Kondo Insulator candidate $SmB_6$

Resistivity measurements on $SmB_6$ are consistent with suggestions that, below 40K, it's a KI. Curiously, however, below 4K the resistivity saturates and plateaus [9]. This plateau suggests that, below 4K, an additional conduction channel is introduced. Sample quality does not appear to impact the plateau,

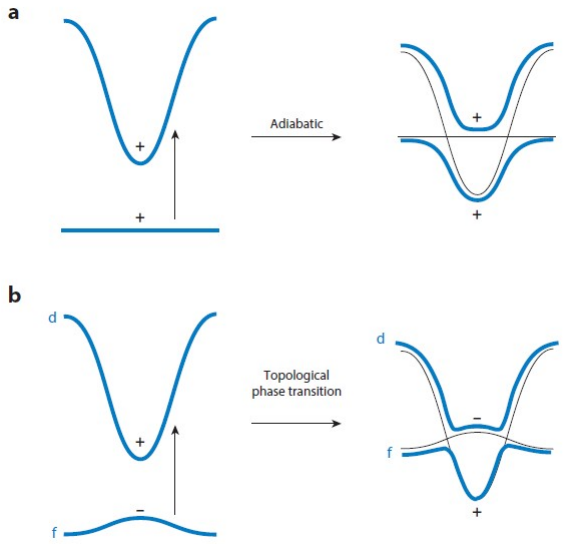


Figure 3.1: Band comparison between a conventional insulator and a Topological Kondo insulator from [9]. Images on the left are of band structures in a non-interacting system, and images on the right are the structures that arise once spin-orbit coupling is turned on adiabatically. As seen in (a), the bands of a conventional insulator have the same parity, and therefore don't cross. However in (b), the bands have opposite parities and are therefore pushed together, leading to band crossing.

and has been an open question under study for roughly the last decade [9]. Measurements on $SmB_6$ have suggested that it may be a TKI ([17], [18], [19], [20]), though at this time there is no "smoking gun" that conclusively indicates that $SmB_6$ is in fact a TKI.

Probing the behaviour of $SmB_6$ using the thermal Hall effect holds strong potential for uncovering whether $SmB_6$ is a TKI. If $SmB_6$ is a TKI, then in the Kondo insulating phase, only surface conduction electrons should be heat current carriers. The problem is that at low temperatures, the longitudinal thermal conductivity of $SmB_6$ is dominated by phonons without an applied magnetic field [2], making it difficult to investigate transport properties of surface states. This phonon contribution to thermal conductivity may be filtered out by performing thermal Hall measurements, providing a channel to investigate possible surface states. However when a magnetic field is applied to $SmB_6$, an additional thermal conductivity channel appears, though it is not clear exactly what is causing this channel [2]. Thermal Hall measurements may provide insight into the nature of this magnetic field induced

thermal conductivity channel.

Quantum oscillations (QO's) have been observed in magnetization measurements of $SmB_6$ [21]. This is a shocking result, as QO's typically only arise in electronically conducting materials, when the Fermi surface is quantized as Landau levels are formed when a magnetic field is applied [21]. This unusual bulk behaviour may be further explored using thermal Hall measurements.

It's clear that the thermal Hall effect may be useful in characterizing such a complex system as $SmB_6$, necessitating the construction of a thermal Hall experimental setup. The following chapters will then be dedicated to detailing the construction and testing of a thermal Hall experimental setup.

# Part II

# Experimental Design, Methods, and Testing Results

# Chapter 4

# Experiment Construction

Performing thermal conductivity measurements has been an established practice in condensed matter physics since the mid 20th century [22], and assembling experimental equipment sensitive enough to detect longitudinal thermal conductivity signals has been well established in our research group for over a decade [1]. However, signals observed in thermal Hall measurements are on average three orders of magnitude smaller than thermal conductivity measurements [23], so there are a number of design considerations to make with respect to accuracy and precision in detecting these small signals.

## 4.1 Probe

The experiment is designed to be performed inside of a probe that's emersed in a bath of liquid cryogens (ie., liquid nitrogen or helium). The full probe (see figure 4.1) is 2m long, with the experiment housed at the tail. Once the vacuum can is attached to the tail of the probe (part H of figure 4.1), a rotary pump can be connected to the vacuum chamber valve (part E of figure 4.1) to pump out the vacuum chamber to a pressure of $\sim 10^{-6}$ mbar.

When the probe is emersed in a liquid helium bath, the base temperature of the system is 1K. This is achieved by leveraging the evaporative cooling power of helium in a component of the probe called the 1K pot. A small and constant flow of liquid helium from the main helium bath is supplied to the 1K pot reservoir (part K of figure 4.1) using a needle valve (part G of figure 4.1) with a fine scale. A vacuum pump is connected to the 1K pot (part E of figure 4.1) to pump on the 1K pot reservoir, evaporating the liquid helium. The liquid helium inlet to the 1K pot and the pressure of the pump are finely tuned to achieve the desired cooling power.

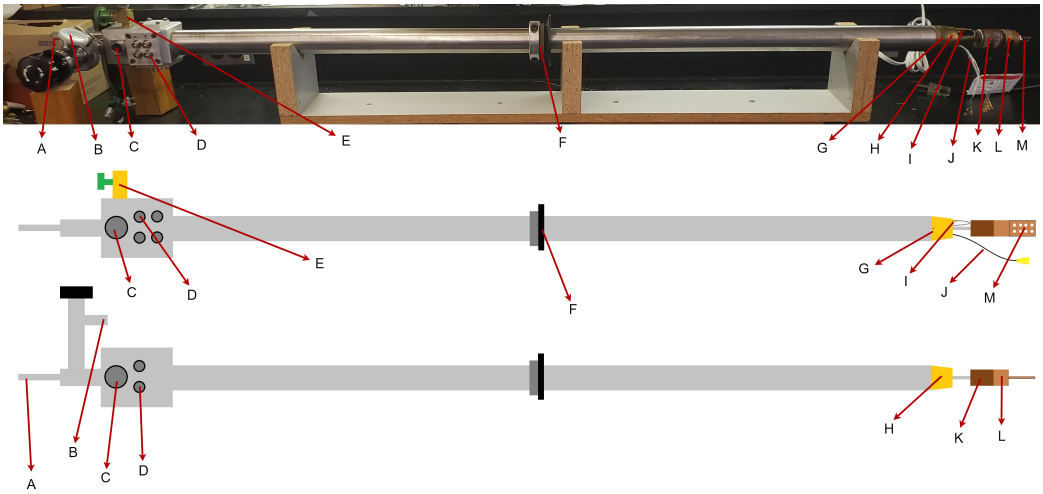


Figure 4.1: Schematic of the full experimental probe. Middle image is a schematic of the probe in the orientation seen in the photo (upper image), lower image is a schematic of the probe rotated 90°to the top of the page. A - Needle valve handle for 1K pot, B - 1K pot pump connection, C - Bulkhead connections for the Lake Shore temperature control (middle) and sample heater (lower), D - Bulkhead connections for capacitors, E - vacuum chamber pumping connection, F - collar that's clamped down onto cryogenic bath, G - 1K pot liquid helium inlet, H - vacuum can connection, I - connection to 1K pot, J - micro coaxial cables for connection to capacitors, K - 1K pot with printed circuit board on exterior, L - thermal sink connected to the Lake Shore temperature control, M - mount for sample puck

### 4.1.1 Connections to Measurement Devices

Figure 4.2 shows a schematic for how the measurement devices required for the experimental setup are connected to the probe. Six BNC cables (one for each capacitor plate) run from the BNC bulkhead connectors on the probe to a multiplexing unit. This multiplexing unit is used to switch the channel that the capacitance bridge is measuring, so that only one capacitance bridge is required in order to perform measurements on three capacitors. The multiplexing unit is then connected to the capacitance bridge.

A multi-channel wire bundle runs from the probe to the Lake Shore temperature controller, for electronic connection to the Lake Shore thermometer and Lake Shore temperature controller heater. Another multi-channel cable bundle runs from the probe to a USB DAQ, which is powered and controlled by a computer.

The magnet is housed inside of the liquid helium bath, a cable bundle runs from bulkhead connections on the liquid helium bath to the magnet controller.

The capacitance bridge, multiplexing unit, and Lake Shore temperature controller are all powered by a transformer, used for the ability to filter noise from a standard North American AC wall power supply. The power transformer is grounded to a water pipe. The magnet controller requires a significant amount of power to operate, so the magnet controller is separately connected to a specialized wall outlet.

The capacitance bridge, Lake Shore temperature controller, and magnet controller are all controlled by a GPIB connection to a computer in a daisy chain.

### 4.1.2 Probe Wiring

Wiring connecting the sample puck to measurement devices runs the full length of the probe, and is thermally anchored to a cold sink close to the tail of the probe. The wiring from the top of the probe to the sample puck used to establish electronic connection to the capacitors are all low temperature micro coaxial cables, two pairs are Belden-E 83265 micro coaxial cables and one pair is Lake Shore CC-SS-25 micro coaxial cables. Wiring for electronic connection of the sample heater and Lake Shore temperature controller (comprised of a resistive thermometer and a resistive heater) are all twisted pairs of silver wire.

At the tail of the probe, the micro coaxial cables terminate at lepra/con female connectors on the sample puck. The Belden-E 83265 cables were installed onto the probe for a previous experimental setup and, to minimize financial costs, were not replaced when the pair of Lake Shore CC-SS-25 micro coaxial cables were installed. Coaxial cables are used for the capacitors so that the capacitance bridge can make 3-wire measurements, as discussed in section 4.7. At the top of the probe, the micro coaxial cables terminate at hermetically sealed BNC bulkhead connectors.

The twisted pair for the sample heater terminate at a pair of male gold pins at the tail of the probe which connect to the sample puck. The Lake Shore thermometer and heater are attached permanently to the probe (see figure 4.1, part L), so the twisted pairs are soldered directly to the thermometer and

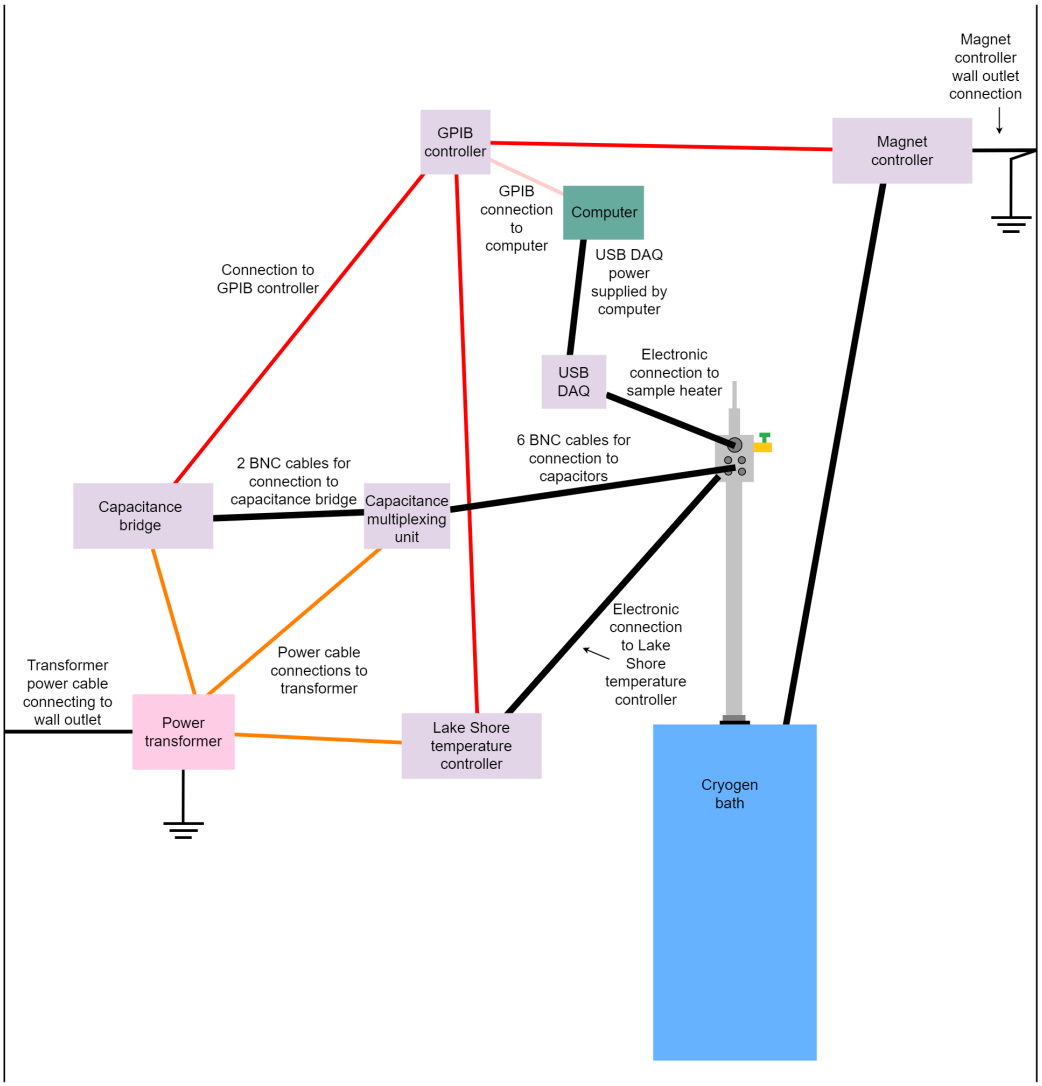


Figure 4.2: Schematic of all equipment required for the experimental setup

heater. At the top of the probe, the sample heater twisted pair terminates at a multi-pin connector. This connector is used in experiments where the sample box as described in [1] is used to perform longitudinal thermal conductivity experiments — electronic connections to the resistive thermometers are maintained using this connector in the longitudinal thermal conductivity experiment. The Lake Shore temperature controller twisted pairs all terminate at a different multi-pin connector at the top of the probe, dedicated to only the Lake Shore temperature controller.

To ensure that only the resistance of the Lake Shore Cernox thermometer is measured and not that of the thermometer in series with the wiring, the Lake Shore temperature controller performs 4-wire resistance measurements on the resistive thermometer. For the sample heater and the Lake Shore temperature controller heater to generate heat, it is only required to apply a current through the resistive chip, thus only 1 set of twisted pairs is required to maintain electronic connection to each heater.

Silver wires are used for the twisted pairs. Silver has a low resistance at low temperatures [24], Johnson-Nyquist noise that the wires are subject to is minimized [25]. This will increase the accuracy of the temperature controller, and since the sample thermometers are calibrated against the Lake Shore thermometer, it is imperative that the Lake Shore thermometer can accurately measure the temperature of the system.

Unwanted heat transfer from warm portions of the probe to the cold end of the probe should also be avoided. From equation 2 it can be seen that the heat input to the sample needs to be known precisely in order to reliably calculate the measured thermal conductivity. If heat leaks into the experiment from the warm end of the probe, this could alter how much heat is input into the sample, causing errors in thermal conductivity calculation. As discussed earlier, all electronic wires and cables within the probe are thermally anchored to a heat sink in the probe. This acts as a pre-cooling stage for the wiring, as the heat sink will be approximately the same temperature as the cryogenics the probe is immersed in.

## 4.2 Sample Puck

The sample puck is made of copper and houses the experiment. This serves two purposes; first, the experiment is mechanically shielded, allowing for the sample to be mounted in one location and safely transported to another [1]. Second, the copper electrically shields the experiment from external electromagnetic radiation.

Electronic connections to the thermometers and sample heater are made using Kapton-Au wires, which will be discussed further in section 4.4. The Kapton-Au wires run from the lepra/con connectors on the inside of the puck to each plate on the capacitors, and from the gold pins to either side of the sample heater. Thermal connections to the sample are made with 25 micron diameter silver wires, with silver paint affixing the thermal connections as

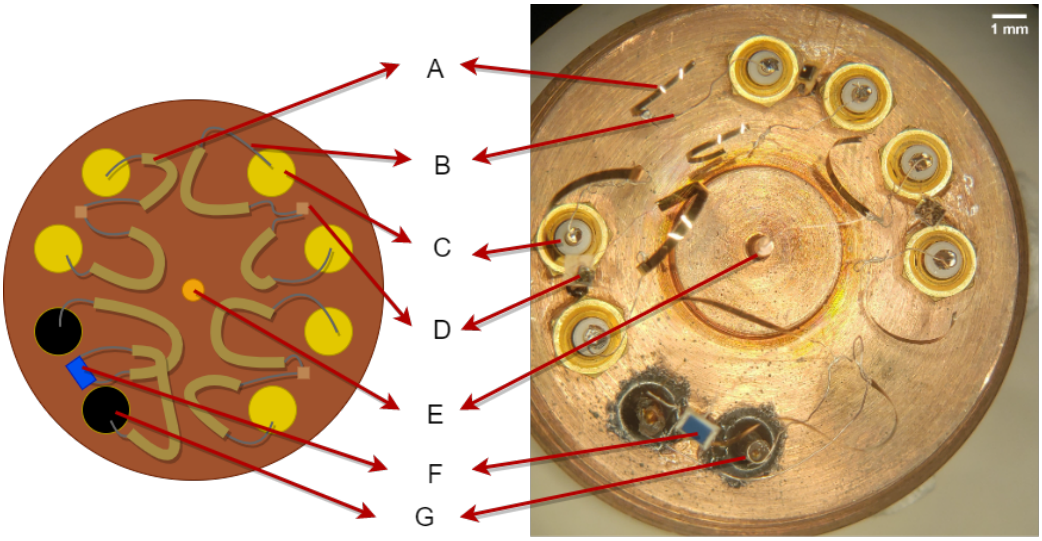


Figure 4.3: Schematic of the sample experimental setup. A - Kapton wires, B - Silver electronic lead to maintain electronic connection between the coaxial connectors/gold pins and the Kapton, and the Kapton and the capacitor plates, C - Coaxial connectors, D - Capacitors, E - Copper heat sink, F - Sample heater, G - Gold pins

desired.

A typical sample will be mounted to the copper heat sink using a copper bracket, as seen in figure 4.4. The sample is attached to the bracket using silver paint, similarly, the bracket is attached to the heat sink using silver paint. The orientation of the sample with respect to the magnetic field may be selected depending on the orientation of the sample as it's attached to the bracket, and the bracket as it's attached to the heat sink. For testing purposes in this work, a sample of silver wire is used, so the wire is attached directly to the heat sink with silver paint, as seen in figure 4.10.

## 4.3 Thermometry

There are several design considerations to be made when determining the thermometry to be used in a thermal Hall experiment. From equation 2, it can be seen that if the temperature gradient $\Delta T$ is not well known, then the thermal conductivity $\kappa$ will also not be well known. Therefore, the thermometers used to measure a temperature gradient need to be able to accurately measure temperature gradients across a sample. There are three types of

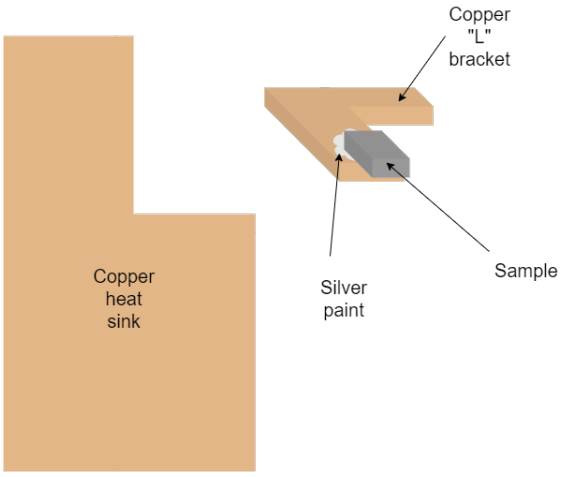


Figure 4.4: Schematic of mounting a typical sample to the heat sink of the sample puck

thermometers that are widely used in thermal Hall experiments.

Thermocouples and resistive thermometers typically have the sensitivity required for thermal Hall measurements, but are also sensitive to magnetic fields. This means that if the experiment is held at a constant temperature, and a magnetic field is applied, the voltage of the thermocouple will change, indicating an apparent change in temperature. The applications of thermocouples and resistive thermometers as well as why they've been ruled out for this work can be seen in appendix D.

### 4.3.1 Capacitive Thermometers

The ideal scenario for thermal Hall measurements would be to use a thermometer that has the sensitivity required to detect a transverse thermal Hall heat current, without being sensitive to magnetic fields. Strontium Titanate (STO) capacitive thermometers fit both of these needs.

Kim *et al.* [23] uses STO thermometers. They evaporated 50nm of gold onto either side of STO wafers to form parallel capacitor plates. The gold plates were additionally covered with silver epoxy, used to bond electric leads to each capacitor plate. They report a temperature resolution of better than 1 part in $10^4$ in the 2K-100K temperature range. For thermal contact to the sample, on each thermometer a silver wire was bonded to the side of the capacitors using GE varnish, to maintain thermal contact but electrical

isolation.

Tinsman *et al.* [26] also uses STO thermometers. They also evaporated gold onto each side of the STO wafers to form capacitor plates, though the gold thickness is not reported. The temperature resolution that they measured was also better than 1 part in $10^4$. The capacitors are encased in an electrically insulating resin, protecting the capacitors from mechanical stress. To maintain thermal contact with the sample, the thermometers were glued to the sample and coated in Type 120 silicone thermal joint compound.

STO is also relatively insensitive to applied magnetic fields. Tinsman *et al.* [26] found that, over a -10T to 10T field sweep at 4.2K, the change in capacitance for one of their thermometers was less than 0.03%. In contrast, an $RuO_2$ resistive thermometer at 4.2K and 10T has a change in resistance of $\sim$0.6% (see figure D.2), and a Cernox resistive thermometer has an apparent change in temperature of $\sim$0.5% at 4.2K and 10T. In other words, the STO thermometers that Tinsman *et al.* fabricated are an order of magnitude less sensitive to magnetic fields than traditional resistive thermometers.

### 4.3.2 Fabrication of STO Capacitive Thermometers

As described at the beginning of this chapter, transverse $\Delta T$ signals are on average three orders of magnitude smaller than their longitudinal counterparts. To satisfy the conditions that the thermometers be insensitive to magnetic field, but sensitive to small changes in temperature, Strontium Titanate (STO) capacitive thermometers are used in this work. The capacitors are formed similar to [23] and [26] by evaporating 100nm of gold onto STO wafers, forming the plates of our parallel plate capacitors, and electrical leads are attached to each capacitor plate with silver epoxy.

The thin film of gold on each side of the STO wafer form two parallel capacitor plates, and the capacitance obeys the following relation:

$$C = \frac{\epsilon A}{d} = \frac{\epsilon_0 k A}{d} \tag{3}$$

Where $C$ is the capacitance, $\epsilon$ is the permittivity of the medium between the capacitor plates, $A$ is the plate area, $d$ is the plate separation, and k is the dielectric constant.

Silver wires of diameter 50 $\mu$m are used to thermally connect each thermometer to the sample. Since the thermal leads from the sample to the

capacitors are silver, they're not only highly thermally conductive but also electronically conductive. To avoid shorting a capacitor plate to the sample, the thermal lead is first affixed to a thin copper plate to conduct heat, and then a GE varnish soaked cigarette paper is used to attach the copper plate to the capacitor. The copper provides thermal conduction, and the GE varnish soaked cigarette paper provides electronic isolation without thermally isolating the lead from the capacitor.

The temperature dependence of the dielectric constant of STO is well known, so changes in capacitance can be used to measure changes in dielectric constant and therefore changes in temperature. The dielectric constant of STO increases by 4 orders of magnitude from room temperature to 1.4K [27], as seen in figure 4.5. In other words, at low temperatures, even small changes in temperature will translate to large changes in capacitance. This implies that small changes in temperature are easy to detect, thus satisfying the condition of sensitivity.

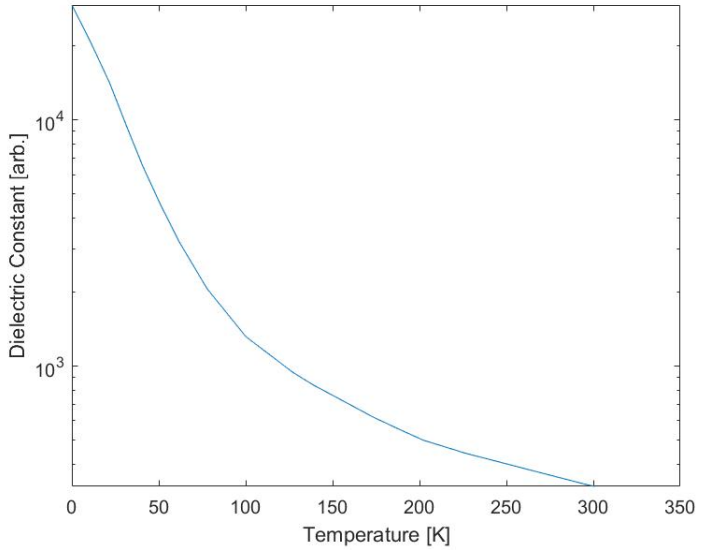


Figure 4.5: Temperature dependence of the dielectric constant of STO from [27]

It's important to note that specific temperature dependences for each thermometer is calibrated *in situ* for each experiment. Tinsman *et al.* [26] notes that each of their thermometers displayed differing temperature dependences, possibly due to varying amounts of heat that the thermometers were exposed

to during their construction. It has also been found [28] that polishing the surface of an STO wafer can drastically decrease the dielectric constant by an order of magnitude, so differing surface treatments can impact the dielectric constant temperature dependence.

## 4.4 Kapton-Au Wires

The Kapton-Au wires are constructed by evaporating a 300 Å thin film of gold onto a 7 $\mu$m thick Kapton sheet. The gold-evaporated sheets are cut to a length to width aspect ratio of approximately 30 using a razor blade. This aspect ratio is chosen to balance the electrical conductivity needs with the thermal resistivity needs. On one hand, the wires are required to be thermally insulating to minimize potential heat leaks. On the other hand, the wires are required to be electronically conductive – a potentially problematic requirement since mobile charge carriers, required for electrical conductivity, are also entropy and thus heat carriers. The thermal resistance of a material is proportional to $\frac{L}{A}$, so the thermal resistance of each wire can be altered with different choices of wire width (impacting the cross sectional area) and/or length.

Further complicating the choice of Kapton-Au wire size is the limited space inside of the sample puck. To increase $\frac{L}{A}$, the length of the wire can be increased and/or the width of the wire can be decreased. Practically speaking, since the wires are cut by hand using a razor, it becomes difficult to cut the wires to a width of less than 0.1 mm. Due to the size of the sample puck, the longest practical length the Kapton-Au wires can be is 10 mm.

Silver electronic leads are attached to the ends of each wire using silver epoxy. To establish electronic connection to the heater and capacitors, two Kapton-Au wires are required for each component — one I+ and one I- for the heater, and one wire for each side of the capacitor plates. One silver electronic lead for each Kapton-Au wire is attached to the required electronic component using silver epoxy, then the other electronic lead is attached using silver paint to the required lepra/con connector for the capacitors, or gold pin for the heater.

## 4.5 Unwanted Heat Transfer

It's important that heat flows only from the heater, through the sample, to the heat sink and thermometers. From equation 2, the thermal conductivity $\kappa$ cannot be determined accurately if the heat supplied to the sample $\dot{Q}$ is not known accurately. It's not possible to measure the exact amount of heat supplied to the sample, only how much heat will be generated by the heater. It is therefore of utmost importance to minimize any possible secondary channels for heat to flow.

Within the sample puck, the sample heater and capacitors are all mounted on small posts made of vespel SP-22, as seen in figure 4.6. The thermal conductivity of vespel SP-22 is small — approximately 3 orders of magnitude smaller [29] than samples typically measured in our research lab [1] at ~4K. Therefore, heat generated by the sample heater will flow most readily through the sample instead of through the vespel SP-22 posts the heater is mounted on.

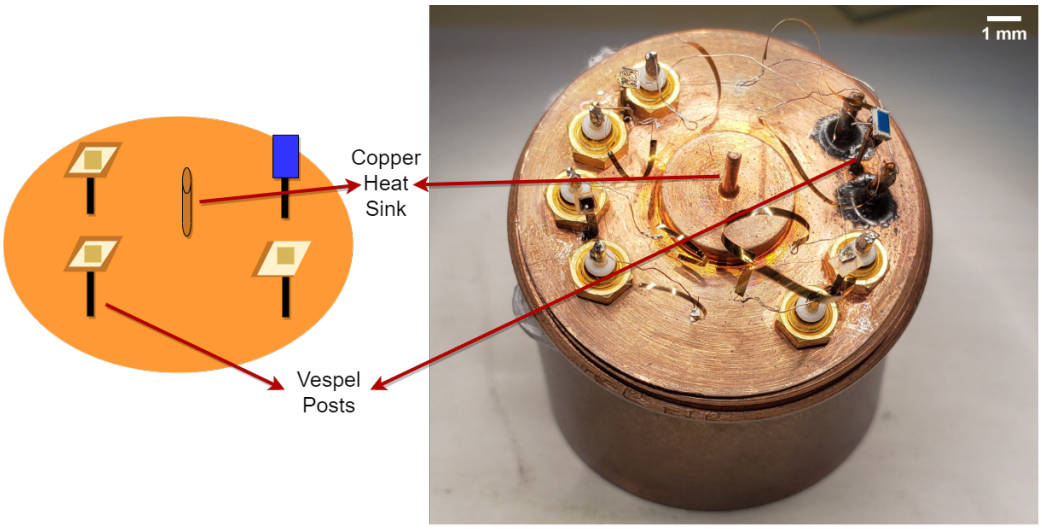


Figure 4.6: A side-view schematic of the sample puck, showing the vespel posts and copper heat sink.

For testing purposes in this work, measurements are performed on a sample of silver wire. A silver sample is used because there's a wealth of experimental data to compare measured thermal conductivity to [30], [31]. Since silver is an electrical conductor, it's thermal conductivity temperature dependence

is governed by the Wiedemann–Franz law:

$$\frac{\kappa}{\sigma} = L_0 T \tag{4}$$

Where $\kappa$ is thermal conductivity, $\sigma$ is electrical conductivity, $T$ is temperature, and $L_0$ is the Lorenz number, a proportionality constant given by:

$$L_0 = \frac{\pi^2}{3}\left(\frac{k_B}{e}\right)^2 = 2.44 \times 10^{-8}\frac{\mathrm{V}^2}{\mathrm{K}^2} \tag{5}$$

Where $k_B$ is Boltzmann's constant and $e$ is the elementary charge.

The goal is for a temperature gradient to be produced across the sample, and for the thermometers to measure this temperature gradient, while keeping the rest of the components in the sample puck at the same temperature as the Lake Shore thermometer. Since the experiment is under vacuum, heat lost via radiation is minimized such that heat is only transferred between experimental components that are in thermal contact.

Once heat is generated by the sample heater, there are other possible channels for the heat to flow; through the electronic connections, and/or through the post that the heater is mounted on. Once heat flows to the sample, there are only two channels for the heat to flow; through the thermal leads to the capacitors, or to thermal ground. This is the desired configuration, as the choice of capacitor/sample heater wiring and mounts can minimize unwanted heat transfers.

The thermal conductance of a material:

$$\sigma = \kappa\frac{A}{L} \tag{6}$$

Can then be used to find the thermal resistance of that material:

$$R = \frac{1}{\sigma} \tag{7}$$

The geometry of the sample, as well as other experimental components, can be seen in table 4.1.
The thermal conductivity of each material (seen in figure A.1) can then be used with the geometries listed in table 4.1 along with equations 6 and 7 to calculate the thermal resistance of each component, which can be seen in

Table 4.1: Geometry of experimental components

| | Length (m) | Cross-Sectional Area ($m^2$) |
|---|---|---|
| Silver sample | $1.99 \times 10^{-2}$ | $1.96 \times 10^{-9}$ |
| Silver thermal leads | $2.00 \times 10^{-2}$ | $1.96 \times 10^{-9}$ |
| Vespel posts | $6.35 \times 10^{-3}$ | $2.95 \times 10^{-7}$ |
| Kapton film | $1.00 \times 10^{-2}$ | $3.50 \times 10^{-9}$ |
| Gold film | $1.00 \times 10^{-2}$ | $1.50 \times 10^{-11}$ |
| Copper plate | $1.40 \times 10^{-4}$ | $7.18 \times 10^{-7}$ |
| GE varnish soaked paper | $5.00 \times 10^{-5}$ | $7.18 \times 10^{-7}$ |

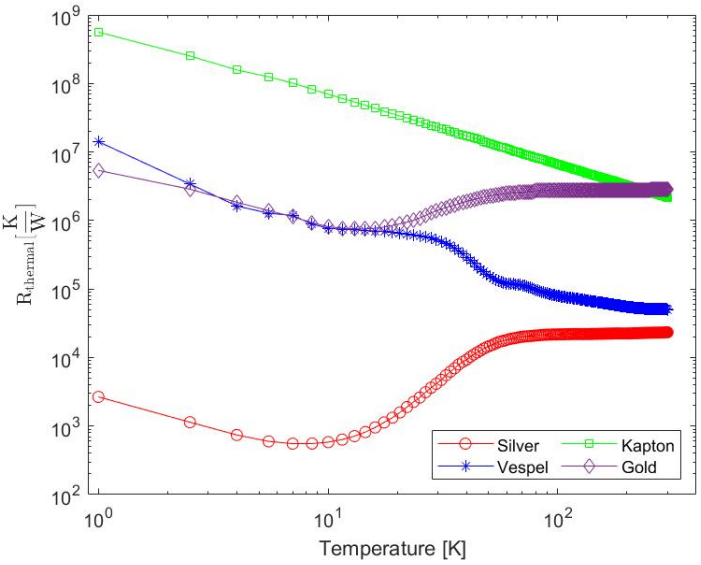


Figure 4.7: Thermal resistance of each original experimental component

figure 4.7.

At the heater and each capacitor, in terms of a secondary heat channel, the vespel post and two Kapton-au wires are in parallel. The thermal resistance of this secondary channel is then found using the following expression:

$$\frac{1}{R_{sec,heater}} = \frac{1}{R_{vespel}} + \frac{1}{R_{Kapton-au}} \tag{8}$$

Where $R_{Kapton-au}$ is found by adding the thermal resistance of the Kapton and gold films:

$$\frac{1}{R_{Kapton-au}} = \frac{1}{R_{Kapton}} + \frac{1}{R_{gold}} \tag{9}$$

Then, using the data from figure 4.7, the ratio of thermal resistance of the silver sample to the thermal resistance of the possible secondary heat channel is calculated and plotted in figure 4.8. In order for heat loses to introduce less than a 1% error, the thermal resistance of the heater secondary channel should be at least two orders of magnitude larger than that of the sample. The temperature range that accurate thermal conductivity measurements can be performed at is also seen in figure 4.7, as the region highlighted in blue.

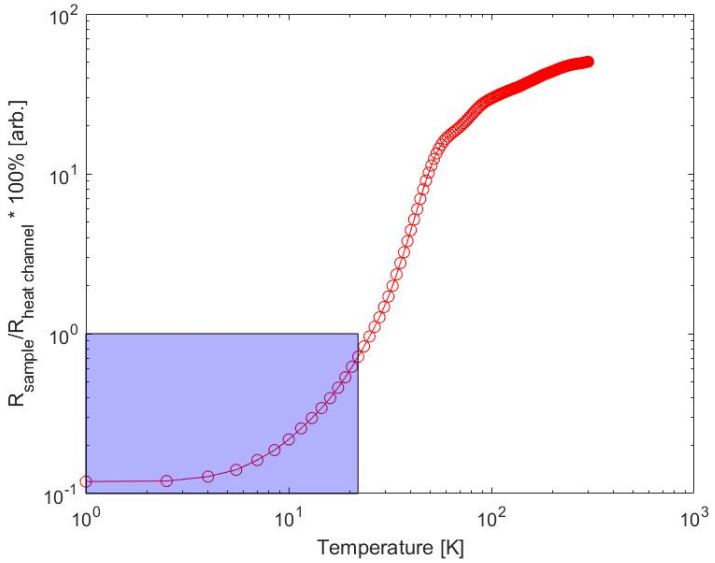


Figure 4.8: Temperature dependence of the ratio $\frac{R_{sample}}{R_{heatchannel}}$, where $R_{sample}$ is the thermal resistance of the sample and $R_{heatchannel}$ is the thermal resistance of 2 Kapton-Au wires and 1 vespel SP-22 post added in series

It's important to note that, as testing results dictate, the dimensions of various experimental components can be altered to change the temperature range at which $\frac{R_{sample}}{R_{heatchannel}}$ is less than 1%. For example, according to equations 6 and 7, if the vespel posts are made thinner and/or longer, the thermal resistance of the posts will increase, which will decrease $\frac{R_{sample}}{R_{heatchannel}}$. This will shift the entire curve seen in figure 4.8 down, increasing the temperature at which $\frac{R_{sample}}{R_{heatchannel}}$ is less than 1%. Alternatively, if a sample is made shorter and thicker, the sample thermal resistance will decrease, decreasing $\frac{R_{sample}}{R_{heatchannel}}$ as well.

## 4.6 Data Acquisition Logic

Software has been written in LabView to acquire data from thermal Hall experiments. The general logic behind thermal conductivity data acquisition is to measure the temperature of the sample before turning on the sample heater, then turn the sample heater on, then measure the temperature at different points along the sample to determine how the sample responded to the applied thermal current. Specifically with thermal Hall measurements, it is necessary to make five thermal connections to the sample: one from the heater to the sample, one from the sample to the heat sink, and one for each of the three thermometers. The placement of the thermal connections for the thermometers is important — "hot" thermometer should be connected close to the heater connection, with two thermometers on the "cold" end, as arranged in figure 4.9. The specific configuration for the silver wire sample used in this work can be seen in figure 4.10.

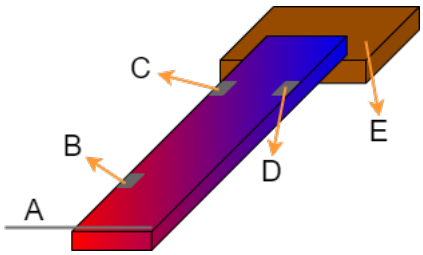


Figure 4.9: Schematic of the sample experimental setup. A - Thermal connection to heater, B - Thermal connection to the longitudinal hot thermometer, C - Thermal connection to the longitudinal cold/transverse hot thermometer, D - Thermal connection to the transverse cold thermometer, E - Copper heat sink

Special care is taken with regards to data acquisition. Since the temperature of the system is controlled by a Lake Shore temperature controller, the temperature will fluctuate slightly about the temperature set-point. Furthermore, when the temperature set-point is changed, the controller will spend some time settling at the new set-point.

It's also necessary to apply a magnetic field to the experimental setup to perform a thermal Hall effect measurement. After changing the magnetic field, the transverse thermal conductivity may also change, so the system will need to be in equilibrium before data may be acquired. The field and temperature dependence of the transverse thermal conductivity of a sample

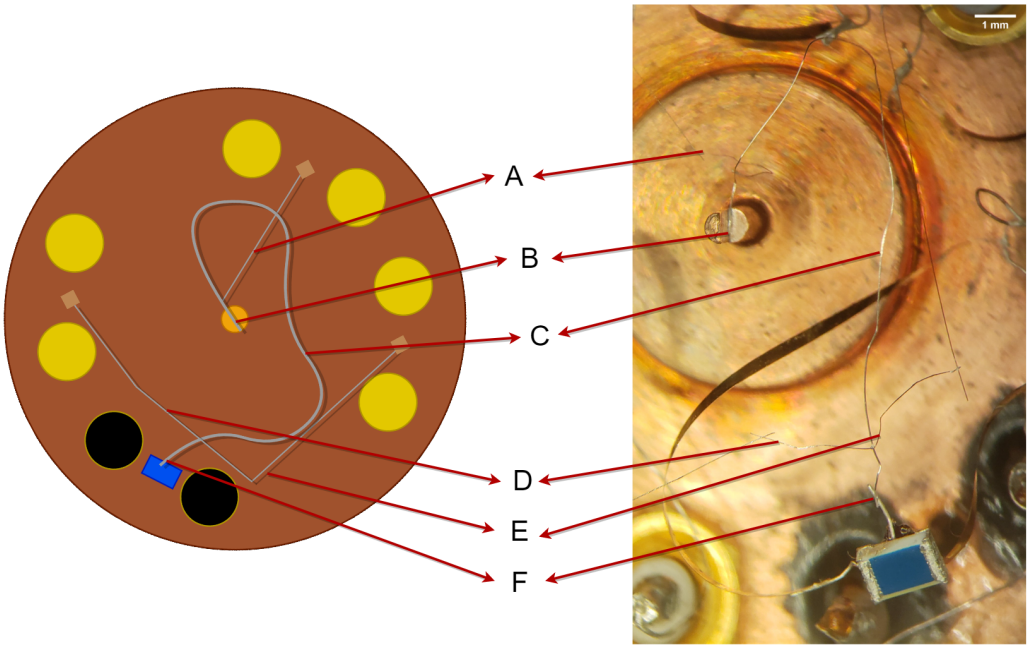


Figure 4.10: Schematic of the silver sample thermal connections. A - Thermal connection to the cold thermometer, B - Copper heat sink, C - Silver sample, D - Thermal connection to one of the hot thermometers, E - Thermal connection to the other hot thermometer, F - Thermal connection to the sample heater

can be investigated using the LabView software developed for this experimental setup. To sweep the temperature dependence, the field is kept constant and the temperature setpoint is changed and to sweep the field dependence, the temperature is kept constant and the field setpoint is changed.

To account for fluctuations, and to ensure that only data taken while the system is in equilibrium is used to compute the transverse thermal conductivity of a sample, data is acquired in four stages, as outlined in figure 4.11. The process for investigating the temperature dependence of the transverse thermal conductivity is outlined below, and a similar process is used to investigate the field dependence.

First, the temperature set-point is changed and the experiment is allowed to come to equilibrium. This is called the heat-off settling time - the Lake Shore temperature and capacitance values of the thermometers are still recorded during this time to monitor the system, but these measurements are not used

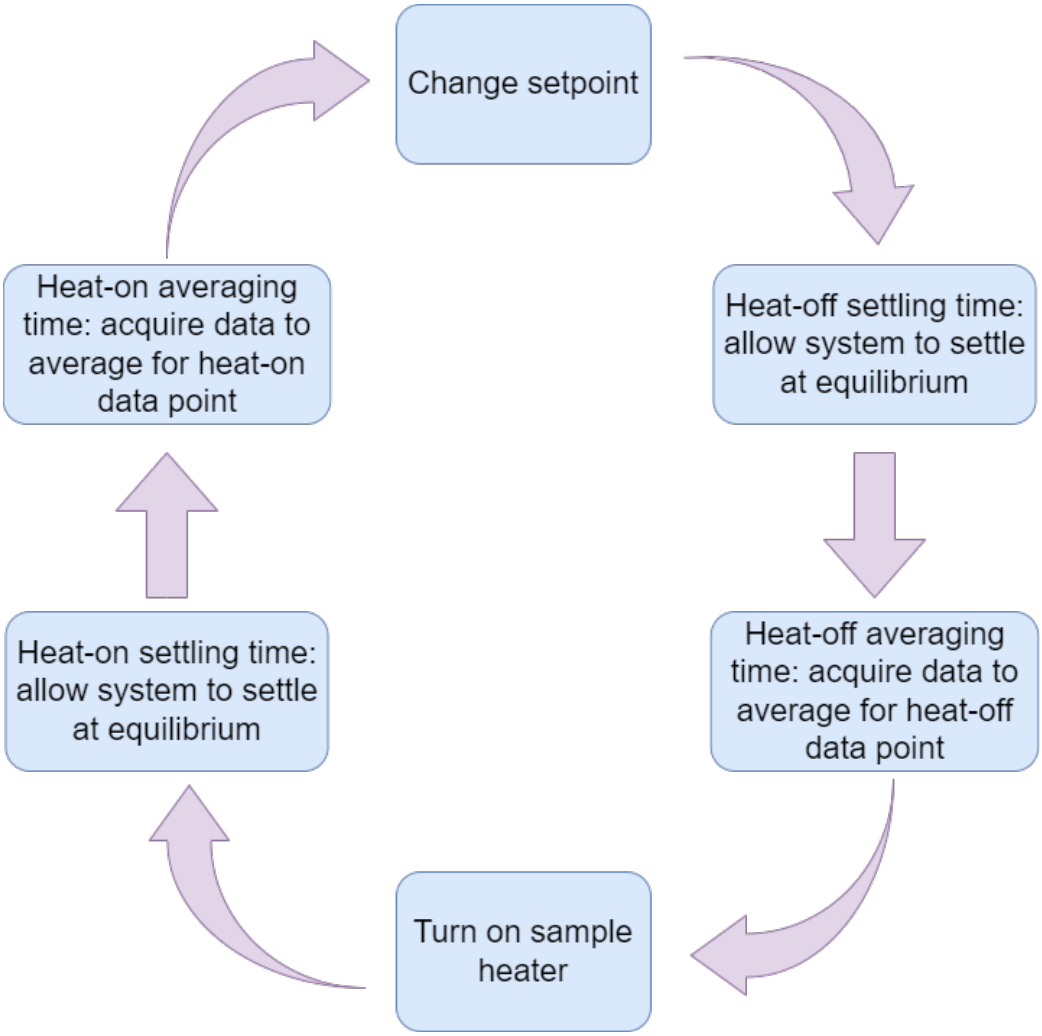


Figure 4.11: Schematic of data acquisition logic

to calculate a thermal conductivity.

Once the system comes to equilibrium, temperature and capacitance data is acquired for a prescribed length of time. This data is averaged over the length of time such that one data point for each of the thermometers, the Lake Shore thermometer, and sample heater voltage is reported. This is called the heat-off averaging time.

Next, the sample heater is turned on. This will of course change the temperature of the sample and sample thermometers, so the system is allowed to come to thermal equilibrium again. Like with the heat-off settling time,

the sensors are all still monitored during this time, but data is not used in thermal conductivity calculations. This is called the heat-on settling time.

Finally, once the system is in thermal equilibrium again, data is acquired for a prescribed length of time. This data is averaged over the length of time such that again, one data point for each of the thermometers, the Lake Shore thermometer, and sample heater voltage is reported. This is called the heat-on averaging time.

The averaged heat-off capacitance measurements are used with the averaged heat-off Lake Shore temperature measurements to produce a polynomial fit of temperature as a function of capacitance for each thermometer. This fit can then be used to convert any measured capacitance value of each capacitor to the corresponding temperature. These calibration curves should be recorded in situ, since slight variations in thermometer fabrication and thermal cycling can impact the exact temperature dependence of each thermometer [26]. However, the overall behaviour of capacitance (increasing as temperature is decreased) remains the same.

## 4.7 Thermometer Resolution

The Andeen-Hagerling 2500A 1kHz Ultra-Precision Capacitance Bridge (AH 2500A bridge) is used to measure the capacitance of each thermometer. This capacitance bridge generates a 1kHz sine wave that excites a ratio transformer, which compares the voltage across the capacitor being measured, and the voltage across a silica-fused capacitor housed within the bridge, in order to determine the capacitance of the unknown capacitor [32].

The bridge can minimize the impact of random noise by internally averaging many measurements to report one data point. Electromagnetic interference will have some oscillating behaviour, and this oscillatory behaviour will average to zero if a sufficiently long averaging time is chosen. In other words, contributions to the measured signal can be minimized if the captured data is averaged. Leveraging the internal averaging abilities of the bridge helps to improve measurement accuracy. The manufacturer reports that, when utilizing the averaging function, the bridge spends proportionally more time settling and preparing for a measurement than it does actually taking the measurement [32]. Therefore, each data point that is averaged will be more accurate than the individual data points that the bridge measures.

Since the bridge uses a 1kHz test signal to perform a measurement, electromagnetic radiation around 1kHz can potentially cause extra electromagnetic noise to be picked up by capacitance measurements. To minimize this problem, the "alternate" feature of the bridge can used. Using this feature, the polarity of the test signal is reversed in a periodic fashion. The bridge can then distinguish between the measurement signal and electromagnetic noise, and can reject the interference signal in measurements.

Coaxial cables are used to take capacitance measurements instead of twisted pairs. This is because, without the shielding provided by the outer conductor of coaxial cables, the bridge will be performing two-wire measurements instead of three-wire measurements. Any cables used to connect a capacitor to the bridge will have some stray capacitance. In a two-wire measurement, this stray capacitance is added to the sample's capacitance in series. If, however, a third wire to ground is added, the bridge can compare the raw measured capacitance with the capacitance of each "side" of the capacitor with respect to ground. The bridge can then measure the stray capacitance of the cables, and remove this from the reported value.

The manufacturer reports that the bridge resolution can detect a change of $10^-7$ pF [32]. To determine if STO thermometers are indeed suitable for detecting transverse $\Delta T$, the bridge's resolution can be compared with the sensitivity of the Tinsman *et al.* STO thermometers. At 4K, Tinsman *et al.* [26] report that their thermometers have a sensitivity of $0.01\ \frac{1}{\mathrm{K}}$, and the raw capacitance of their thermometer is $\sim$55pF. The capacitance bridge therefore has the resolution to detect a change in temperature of 1 part in $10^6$.

In order to detect transverse thermal Hall currents, our thermometers need to be sensitive enough to detect transverse temperature gradients. However this is not the full picture — temperature fluctuations and electronic noise also play a role in the ability to detect these signals. Tinsman *et al.* [26] report a transverse temperature gradient of 1 part in $10^3$, so electronic noise in thermal Hall measurements cannot be larger than 1 part in $10^4$. The capacitance bridge has the resolution to detect these signals, but this assumes that the experiment is not subject to any electronic noise. Testing the thermometer resolution is the focus of chapters 5 and 6.

It's important when investigating electronic noise to consider that, from sections 4.1 and 4.2, it can be seen that the electronic connections to the capacitors are only shielded from the bulkhead connectors at the top of the probe to the sample puck. Once inside the puck, the electronic connection to

each capacitor from the coaxial connection is unshielded. This means that the Kapton-Ti/Au wires actually appear in series with the capacitor when a measurement is performed. Therefore, any stray capacitance and noise in that stray capacitance measurement originating from the wires will be added in series with capacitance measurements of the capacitor itself.

All capacitance measurements performed for this work were taken using the capacitance bridge's "6" averaging setting. This means that 16 samples are taken, each sample being having a duration of 0.1 seconds, and averaged together.

# Chapter 5

# Full Apparatus Testing

As discussed in section 4.5, a silver wire sample was used for testing, because there's a wealth of data to compare measurements with [31], [24]. Additionally, the thermal resistance at liquid helium temperatures is small compared with the thermal resistance of possible secondary heat channels.

## 5.1 Preliminary Room Temperature Testing

Before testing at liquid nitrogen temperatures, the sensitivity of the thermometers was tested at room temperature. At ambient lab temperature, the capacitance of each thermometer and the lab temperature (measured by the Lake Shore temperature controller) were recorded over 3.5 hours. The lab temperature fluctuated by 1K over this time, and the capacitance of each capacitor also changed as a result. The sensitivity $\frac{\Delta C}{C}$ ($\Delta C \equiv \frac{dC}{dT}$) was calculated for each capacitor and averaged over the 3.5 hour run. It was found that the capacitors each had a sensitivity of 0.003 $\frac{1}{\mathrm{K}}$. In other words, at 295K, a 1K change in temperature corresponds to a 0.03 pF change in capacitance.

This is comparable to data from Tinsman *et al.* [26] (see fig. 5.1). It's important to note that the Tinsman *et al.* [26] data only captured thermometer sensitivity up to ∼200K. From equation 3, it can be seen that the dielectric constant of STO is proportional to the capacitance. From figure 4.5, it can be seen that, from 300K to 4K, the dielectric constant of STO and, therefore the capacitance of STO capacitors, increases by 8496%. Additionally, between 300K and 77K, the dielectric constant of STO increases by 550%, but between 300K and 200K, the dielectric constant only increases by 57%. Thus, while Tinsman *et al.* 's 200K data is not an exact one-to-one

comparison, for preliminary testing purposes it does provide a rough order of magnitude comparison.

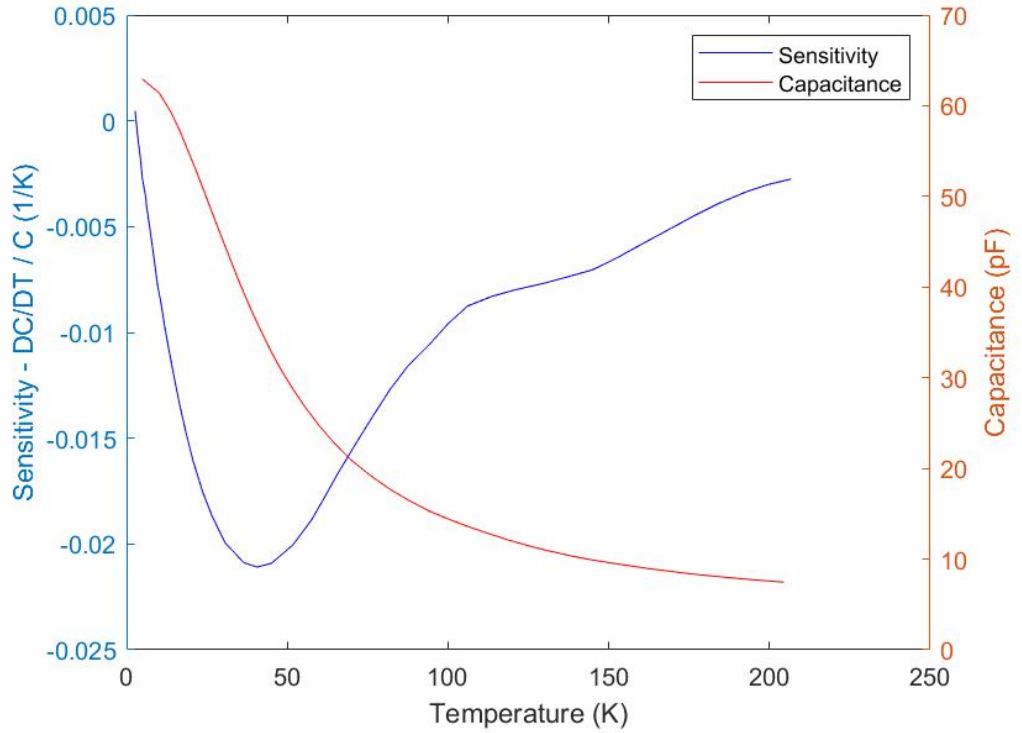


Figure 5.1: Capacitance and thermometer sensitivity of an STO thermometer from 200K to 1K from [26].

From figure 5.1, it can be seen that the sensitivity of their STO thermometer is $\sim$0.0025 $\frac{1}{\mathrm{K}}$ at 200K. This is comparable with the measured sensitivity of this work of 0.003 $\frac{1}{\mathrm{K}}$. Additionally, this suggests that the thermometers are responding as expected to changes in temperature.

## 5.2 Liquid Nitrogen Testing

As discussed in section 4.5, with this experimental setup and with this silver sample, it is not possible to accurately measure the thermal conductivity of the silver sample at liquid nitrogen temperatures. However, it is important to complete preliminary testing of the capacitive thermometers at liquid nitrogen temperatures. It's prudent to complete any necessary troubleshooting

at ∼77K as liquid nitrogen is significantly cheaper than helium, and therefore operating costs associated with having to thermally cycle the experimental setup will be minimized.

### 5.2.1 Thermometer Sensitivity

At liquid nitrogen temperatures, the sensitivity and thermometer resolution can be studied. Using the experimental logic as outlined in section 4.6, the sensitivity of each thermometer is calculated using the heat-off data points. The thermometers' sensitivities at liquid nitrogen temperatures are plotted in figure 5.2.

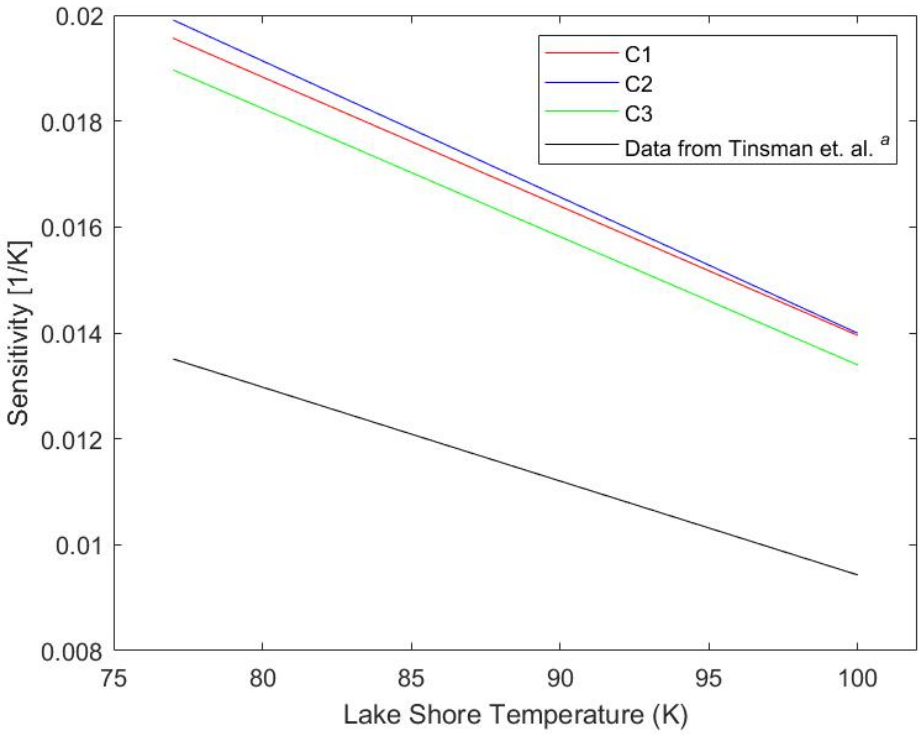


Figure 5.2: Measured STO capacitive thermometer sensitivities in the 77K-100K temperature range. For clarity, the absolute value of the thermometer sensitivity is plotted.

[a] data taken from [26]

The overall behaviour of the thermometers is the same as that of data from Tinsman *et al.* [26]; the sensitivity is increasing linearly with decreasing

temperature in the temperature range of 77K to 100K. However, while the order of magnitude is the same, it's also seen that the sensitivity of the thermometers from this work is higher than the Tinsman *et al.* [26] thermometer.

The increase in sensitivity may be explained by a difference in thermometer preparation techniques. For example, the thermometers fabricated by Tinsman *et al.* [26] may have been exposed to different thermal cycling during fabrication compared to the thermometers fabricated for this work. This may shift the peak sensitivity that is observed in figure 5.1 [26].

There is also a difference of wiring between this work and the Tinsman *et al.* thermometers. They used phosphor bronze wires to provide electronic connection to each capacitor plate, whereas the thermometers of this work are of course wired with Kapton-Au wires. Using the thermal conductivity of phosphor bronze at ∼100K [33], the reported wire diameter of 25 $\mu$m [26], and an estimated wire length of 6 mm (from figure 1 in [26]), the thermal resistance of the phosphor bronze electronic leads is $3.73 \times 10^5 \ \frac{\mathrm{K}}{\mathrm{W}}$, which is an order of magnitude smaller than the Kapton-Au wires as outlined in figure 4.7.

Though this is only an estimate as the wire length is not reported in [26], it's worth noting that the difference in wire materials may impact thermometer resolution and thus may be contributing to the difference in sensitivity between [26] and this work. In order to fully explore this difference in sensitivity, the temperature dependence of the thermometers (and therefore, of their sensitivity) should be measured down to the base operating temperature of the cryostat of 1K.

At ∼100K, with a sensitivity of ∼0.015 $\frac{1}{\mathrm{K}}$ and a bridge resolution of $10^{-7}$ pF, the temperature gradient resolution of the capacitive thermometer is a temperature change of 1 part in $10^6$. However, this does not include the impact that electronic noise has on capacitance measurements, so the overall thermometer resolution should be evaluated with respect to noise.

### 5.2.2 Thermometer Resolution

To analyse the thermometer resolution at liquid nitrogen temperatures, the electronic noise for a heat-off averaged data point is examined. The difference between the raw capacitance measurements and the averaged capacitance measurement for one heat-off averaging step is taken, as seen in figure 5.3.

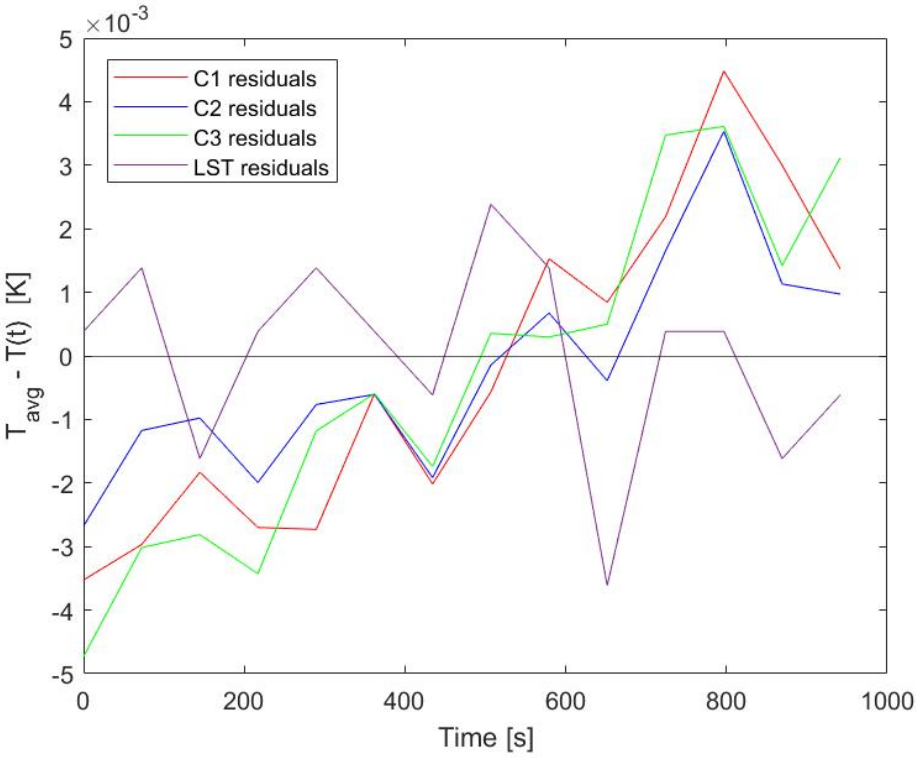


Figure 5.3: Temperature residuals for each capacitive thermometer and the Lake Shore thermometer over a 95K heat-on averaging step. Residuals are calculated as the difference between the average temperature and the real-time temperature.

At 95K, the noise resolution is 1 part in $10^4$. So at liquid nitrogen temperatures, the thermometers have the resolution to measure transverse temperature gradients. Recall from section 4.7 that in order to accurately measure a transverse thermal gradient, the thermometer resolution should be at least 1 part in $10^4$, so at liquid nitrogen temperatures, this condition is satisfied.

## 5.3 Further Testing

After successfully completing liquid nitrogen temperature testing, liquid helium testing was attempted. Several problems with experimental components were revealed in this attempt. It was determined that, after thermally cycling the experiment, the evaporated gold capacitor plates on C2 had become discontinuous. The capacitor was soaked in a 50/50 mixture of ethanol and toluene to remove gold that was not well-adhered to the surface, then more

gold as evaporated onto either side of the capacitor.

Once gold was re-evaporated onto C2, instead of attaching the Kapton wires to each plate via a silver electronic lead and silver epoxy, the Kapton wire was connected directly to each capacitor plate via silver epoxy (see figure 5.4). This was done to remove two joints that could potentially mechanically fail (a joint connecting a silver lead to the capacitor plate, and a joint connecting the silver lead and the Kapton wire).

A second STO thermometer was fabricated with the new C2. While making changes to components inside of the sample puck, C1 was damaged and replaced with this newly fabricated capacitor.

It was also determined that the Kapton-Au wires connecting C3 were not maintaining sufficient electrical connection to each capacitor plate for the capacitance bridge to take a capacitance measurement. To examine the behaviour of the capacitor without the Kapton-Au wires, the wires were replaced with PtW coils. This is the material used in longitudinal thermal conductivity experiments in our research group [1] to provide electrical connection to thermometers while maintaining thermal isolation.

### 5.3.1 Testing PtW-Wired Capacitor

Once the capacitors were replaced and re-wired, the thermometer resolution of the modified experimental components was tested at liquid nitrogen temperatures. At this testing stage, the capacitors are labelled as follows:

- C1 - The longitudinal "hot" thermometer. Kapton-Au wires connected as seen on the right of figure 5.4
- C2 - The longitudinal "cold" thermometer and the transverse "hot" thermometer. Kapton-Au wires connected as seen on the right figure 5.4
- C3 - The transverse "cold" thermometer. PtW coils connected using the same technique as seen on the left of figure 5.4

However, upon cool-down, electronic connection to C1 was lost. The electronic noise of C3 is then compared only to C2, as seen in figure 5.5. The noise resolution of C2, C3, and the Lake Shore thermometer are all 1 part in $10^4$, with the magnitude of noise on C3 being slightly less than that of C2.

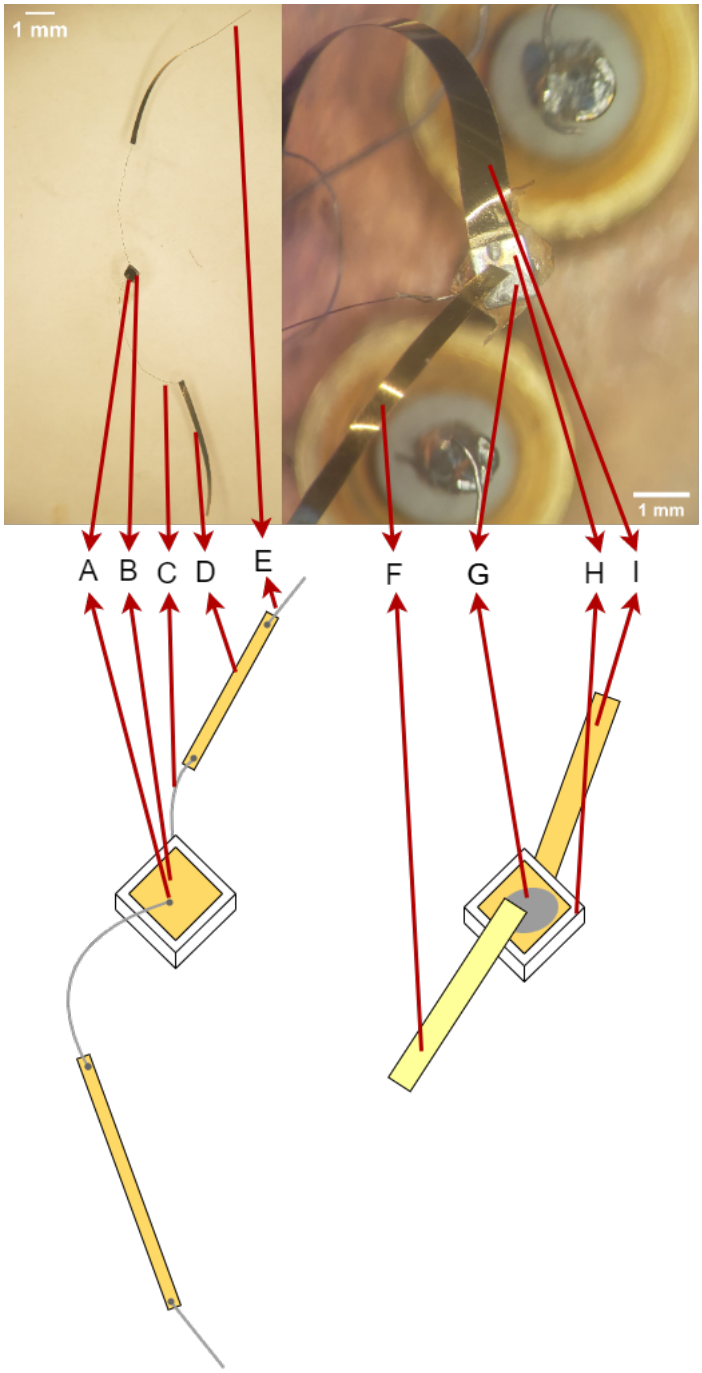


Figure 5.4: A comparison of two methods for electrically connecting an STO thermometer to Kapton-au wires. Left - silver electronic leads are connected to each capacitor plate via silver epoxy, right - Kapton-au wires connected directly to each capacitor plate via silver epoxy. A - Silver epoxy joint between Kapton-au electronic lead and capacitor plate, B - STO capacitor, C - Electronic lead between Kapton-au wire and capacitor plate, D - Kapton-au wire, E - Electronic lead between Kapton-au wire and coaxial connector, F - Kapton-au wire, Kapton side facing camera, G - silver epoxy joint between the gold side of the Kapton-au wire and capacitor plate, H - STO capacitor, I - Kapton-au wire connected to bottom plate, gold side facing camera.

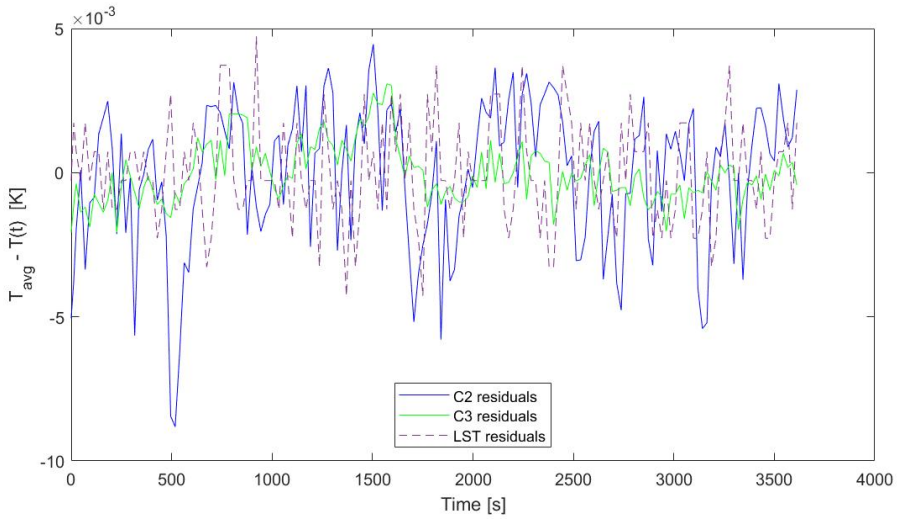


Figure 5.5: Noise comparison at ∼100K between a Kapton-Au wired capacitor and PtW wired capacitor. "Noise" is calculated by taking the difference between the averaged temperature and instantaneous temperature measurement

Previous preliminary measurements on Kapton-Ag have shown that using Kapton-Ag wires to maintain electronic connection with ruthenium oxide resistive thermometers decreases the electronic noise compared with PtW wires. A noise comparison between the Kapton-Ag wired resistive thermometer, PtW wired resistive thermometer, and the Lake Shore temperature controller resistive thermometer can be seen in figure 5.6.

Note that the resolution of the resistance measurements is 0.01Ω and that a background linear temperature drift was subtracted from this data. The portions of each curve that see a gradual linear slope are artifacts of the background data being subtracted — in the original data (seen in appendix B), these portions appear as regions of data where the resistance is unchanged. The portions of each curve that see vertical fluctuations are artifacts of the resistance bridge's resolution. In other words, noise experienced during these measurements may be smaller than changes in resistance that the resistance bridge can resolve. For further information on the Kapton-Ag wires, see appendix B.

It can be seen that there is some discrepancy between the noise displayed in figure 5.5 and figure 5.6. The former shows that a Kapton wired thermometer experiences more electronic noise than a PtW wired thermometer, while

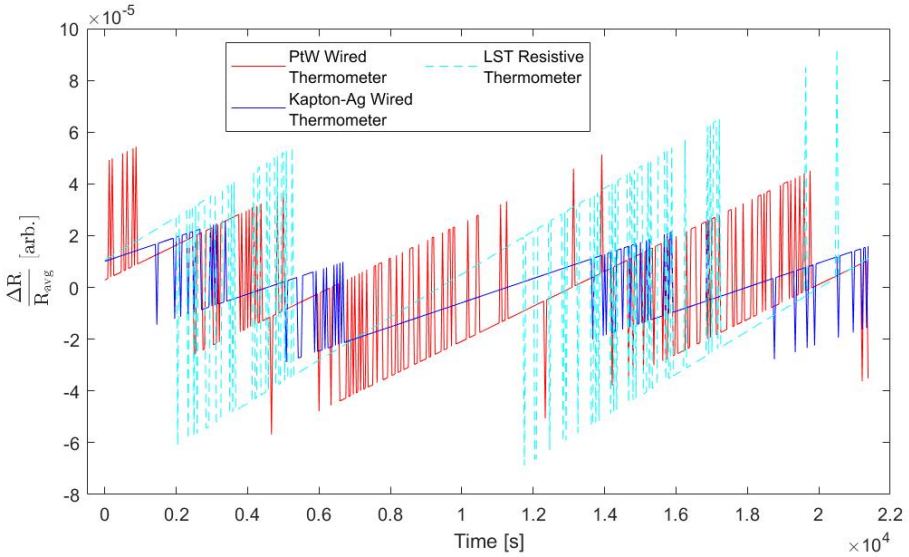


Figure 5.6: Noise comparison at 77K between a Kapton-Ag wired resistive thermometer, a PtW wired resistive thermometer, and the Lake Shore temperature controller resistive thermometer. "Noise" is calculated by taking the difference between the averaged temperature and instantaneous temperature measurement. Note that during data collection, there was a linear temperature drift, as illustrated by figure B.1. The background linear fit was subtracted from the raw data, and this subtracted data is used to quantify noise.

the latter shows that a Kapton wired thermometer experiences less electronic noise than a PtW wired thermometer at liquid nitrogen temperatures.

Since the thermal resistance of PtW is ∼2 orders of magnitude smaller than the Kapton-Au wires (see figure B.2), the expectation is that the Kapton-Au wires would be less noisy. Additionally the PtW coils, by nature of being electrically conducting coils in an AC circuit, will introduce some stray inductance in each measurement that would present as some fluctuation about an average measured value. The coiled geometry was chosen to increase the length of each PtW wire, which from equations 6 and 7 increased thermal resistance, so stray inductance is an inevitable complication of using PtW coils for wiring. Since the Kapton-Au wires are flat, they do not introduce any stray inductance, so the expectation is that they would be less electronically noisy than the PtW coils.

It's important to note that previous data collected for Kapton-Ag wires and

PtW coils was collected using a 17 Hz resistance bridge. In contrast, data for Kapton-Au wires and PtW coils in this work was collected using a 1kHz capacitance bridge. There may be some measurement subtleties that help explain why Kapton wires are less noisy than PtW coils in one experimental setup and not the other, though this requires further investigation.

There is however one more possibility for why the Kapton-Au wires in this work experience more electronic noise than PtW coils, and that is the method of adhering gold to the surface of Kapton. If the gold is not well-adhered to the Kapton substrate, there may be some gold delamination on portions of the gold film, introducing electronic noise as the gold film is no longer one continuous layer.

### 5.3.2 Exploring Gold Adhesion

It appears as though the evaporated gold used to form the capacitor plates, and the evaporated gold on the Kapton-au wires, may not be well adhered to the capacitors and Kapton respectively. There are two pieces of evidence to support this claim.

First, even though C1 and C2 were fabricated using identical methods, electronic connection to C1 was lost during a cooldown while electronic connection to C2 was maintained. Then, while warming the experiment up back to room temperature, electronic connection to C1 was suddenly established again. This is a consistent result regardless of wiring outside of the sample puck.

This indicates that, somewhere between the coaxial connector on the inside of the sample puck and C1, electronic connection to C1 is being lost. This isolates the problem to the Kapton wires and capacitor plates - both of which rely on evaporated gold to maintain electronic connection.

Second, the Kapton wired thermometer in this work experienced more electronic noise than the PtW wired thermometer. This contradicts previous preliminary data that was captured on resistive thermometers, showing a reduction in noise by using Kapton wires. If the Kapton wire on C2 has portions of gold that are not well adhered to the Kapton, but not enough for the gold to become completely discontinuous on the axis of current flow, the total capacitance of the wires and capacitor in series may be varying measurement to measurement, depending on how much gold is in electrical contact.

The current construction of the Kapton-au wires consists simply of gold evaporated onto a sheet of Kapton (with electronic leads attached to the gold via silver epoxy). Similarly, the capacitor plates are formed by evaporating gold directly onto each side of an STO wafer. However, gold does not adhere well to insulating materials [34], so an adhesion layer may improve the Kapton-Au wire and gold capacitor plate lifetime and performance. The use of a Ti adhesion layer on the Kapton and STO is explored in chapter 6.

# Chapter 6

# Gold Evaporation Complications

Gold is difficult to adhere to surfaces due to it's low chemical reactivity [35]. Originally, to form the STO capacitors and the Kapton-Au wires, gold was evaporated directly onto the STO wafers and Kapton film. No other treatments were done to ensure the gold stayed well adhered. Since gold does not adhere well to surfaces, the gold films evaporated onto the STO and Kapton were delicate and prone to delamination, causing performance issues with the capacitor and wires [35]. Therefore, it appears that the most likely source of failure of the capacitors and Kapton-au wires is the untreated evaporated gold.

To circumvent this problem, it is common practice to use a metallic adhesion layer in between gold and substrate if the substrate is electrically insulating [34], [36]. Titanium is commonly used as an adhesion layer, as it has a favourable chemical reactivity, so titanium deposited onto the STO or Kapton substrate bonds readily to the substrate and to the gold overlayer [35].

Some $TiO_2$ is formed during titanium deposition (caused by water adsorbed on the substrate), however the titanium by and large remains an amorphous layer. Evaporated gold is then bonded to the titanium surface, and measurements have shown that the number of gold nucleation sites increases dramatically when compared with gold evaporated directly onto a $SiO_2$ substrate [35]. In other words, gold adheres far better to the surface with a titanium adhesion layer than directly to the substrate surface. A schematic of this model is seen in figure 6.1.

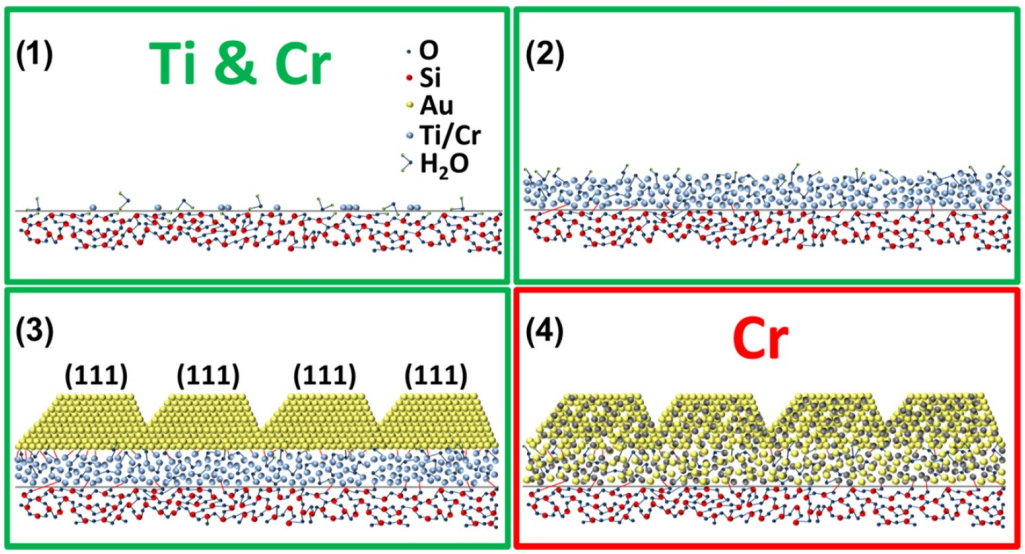


Figure 6.1: Schematic of a titanium adhesion layer from [35]. (1) before an adhesion layer is applied, there may be water adsorbed on the substrate surface, (2) Ti is deposited on the substrate surface, bonding with the substrate and forming some $TiO_2$, (3) Au is them deposited on the Ti layer, bonding with the Ti without any Au or Ti interlayer diffusion, and (4) schematic of a Cr adhesion layer demonstrating Cr/Au interlayer diffusion.

## 6.1 STO and Kapton Preparation

The STO wafer used for testing this new Ti/Au evaporation method had previously already had a layer of gold evaporated on either side to form gold capacitor plates. A 50/50 mix of ethanol and toluene was used to remove any gold that was not well-adhered to the surface. This still leaves behind some gold that is still well adhered to the wafer, however for preliminary testing purposes, cleaning the surface of the wafer to this degree is sufficient.

The edges of the STO wafer were taped with Kapton tape to prevent either titanium or gold from encroaching onto the wafer edges, which could cause the capacitor plates to short. Both sides of the wafer had 20 nm of titanium, then 60 nm of gold evaporated onto the surface. These are the standard thicknesses chosen by our collaborators for Ti/Au evaporation. In particular, a Ti layer thickness of 20 nm is chosen to ensure that the Ti forms a continuous film.

To prepare the Kapton for Ti/Au evaporation, Kapton film was taped to

a glass slide using Kapton tape. A 20 nm layer of Ti and an 80 nm layer of Au were then evaporated onto the Kapton film. A 7 $\mu$m thick Kapton film was originally intended to be used, similar to the Kapton-Au wires described in section 4.4. This thickness was chosen to provide a favourable thermal resistance for the Kapton-Ti/Au wires. From equations 6 and 7, thermal resistance is inversely proportional to cross sectional area, which is in turn proportional to thickness. Therefore, minimizing the Kapton film thickness will maximize thermal resistance. However, due to a small oversight, a 50 $\mu$m Kapton film was used instead. As a result, heat loss estimates from section 4.5 will be altered, with updated geometries listed in table 6.1.

Table 6.1: Updated geometry of experimental components

| | Length (m) | Cross-Sectional Area ($m^2$) |
|---|---|---|
| Silver sample | $1.99 \times 10^{-2}$ | $1.96 \times 10^{-9}$ |
| Silver thermal leads | $2.00 \times 10^{-2}$ | $1.96 \times 10^{-9}$ |
| Vespel posts | $6.35 \times 10^{-3}$ | $2.95 \times 10^{-7}$ |
| Kapton film | $6.17 \times 10^{-3}$ | $2.5 \times 10^{-8}$ |
| Titanium film | $6.17 \times 10^{-3}$ | $1.00 \times 10^{-11}$ |
| Gold film | $6.17 \times 10^{-3}$ | $3.00 \times 10^{-11}$ |
| Copper plate | $1.40 \times 10^{-4}$ | $7.18 \times 10^{-7}$ |
| GE varnish soaked paper | $5.00 \times 10^{-5}$ | $7.18 \times 10^{-7}$ |

Using the geometries listed in table 6.1 with the thermal conductivities shown in figure A.1 and equations 6 and 7, the updated thermal resistance of each experimental component is seen in figure 6.2.

Since the experimental setup will eventually be used to study more complex systems than silver, it's prudent to compare the thermal resistance of the secondary heat channel to the thermal resistance of a typical sample of interest. This comparison is completed for the thinner Kapton-Au wires and thicker Kapton-Ti/Au wires. For this, $LaB_6$ is used. The thermal resistance of $LaB_6$ is calculated using thermal conductivity data from [37] and [38]. An $LaB_6$ sample that the research group has on hand has dimensions of 9.88 mm x 0.2 mm x 0.3 mm.

The temperature dependence of $\frac{R_{sample}}{R_{sec.heatchannel}}$ from 300K down to 1K is plotted in figure 6.3. It can be seen that below 4K, if the thicker Kapton-Ti/Au wires were to be used, $\frac{R_{sample}}{R_{sec.heatchannel}}$ would be greater than 1%. Therefore, the thicker Kapton-Ti/Au wires will be used for preliminary testing of the newly fabricated STO capacitor with a Ti adhesion layer, but these thicker

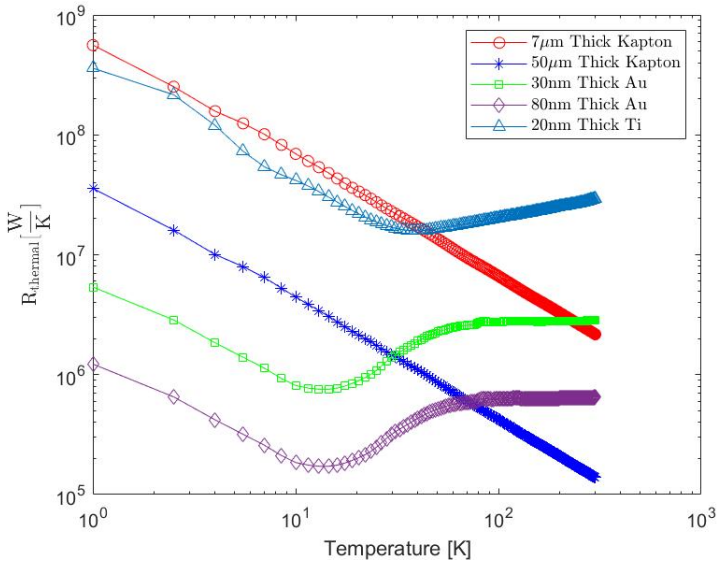


Figure 6.2: Thermal resistance of new experimental components (ie., thicker Kapton, addition of Ti layer, thicker Au layer)

wires will need to be replaced with 7 $\mu$m thick Kapton-Ti/Au wires in order to accurately perform thermal Hall measurements.

With the newly fabricated STO capacitor (fabricated with the thicker Kapton-Ti/Au wires), the three capacitors are now labelled as follows:

- C1 - The longitudinal "hot" thermometer. This capacitor has a Ti adhesion layer to keep the Au capacitor plates well adhered to the STO wafer. Kapton-Ti/Au (50$\mu$m thick Kapton) wires connected as seen on the right of figure 5.4
- C2 - The longitudinal "cold" thermometer and the transverse "hot" thermometer. Kapton-Au wires connected as seen on the right figure 5.4
- C3 - The transverse "cold" thermometer. PtW coils connected using the same technique as seen on the left of figure 5.4

At the liquid nitrogen testing phase, it was discovered that the new Kapton-Ti/Au wires were too thick for the default excitation voltage of the capacitance bridge to be used. This can be seen as a result of equations 6 and 7 — by increasing the Kapton thickness, the thermal resistance of the Kapton-Ti/Au wires is decreased. In other words, the thicker Kapton-Ti/Au wires

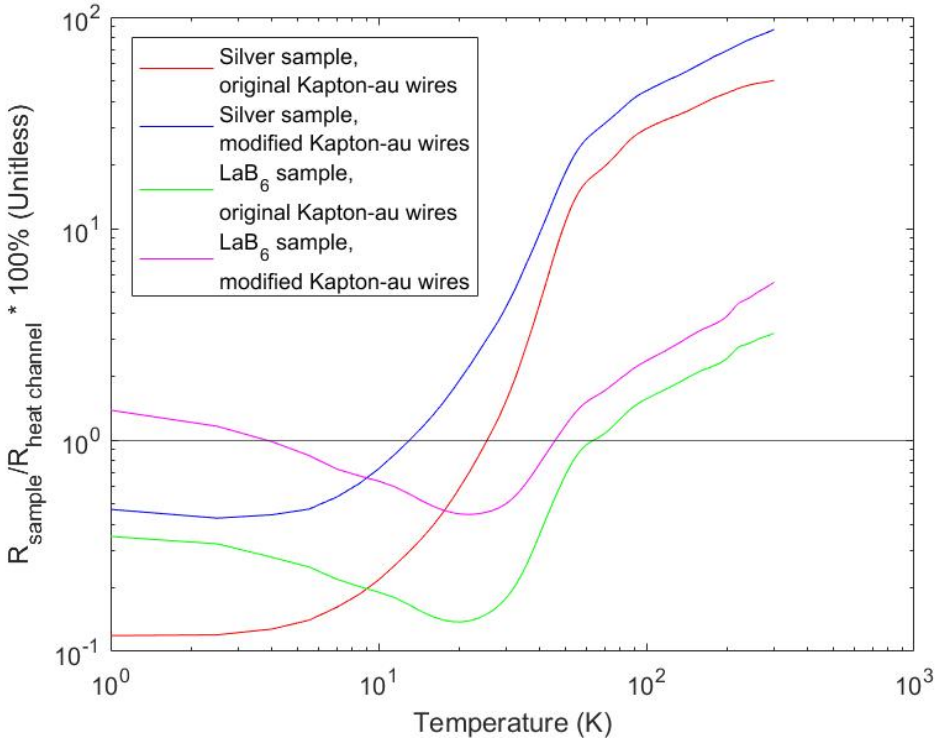


Figure 6.3: Temperature dependence of $\frac{R_{sample}}{R_{sec.heatchannel}}$ for various experimental setups.

will allow for more unwanted heat transfers from the electronic wiring to the capacitor, causing measurements to deviate from an average measured value.

The thermal resistance of both sets of Kapton wires is seen in figure 6.5, showing that the thermal resistance of the thicker Kapton-Ti/Au wiring has decreased by approximately a factor of 4. While it's true that only the Ti/Au layer is electrically conducting, this layer is in thermal contact with the Kapton film. The Ti/Au layer experiences Joule heating when an electronic current is applied across it, which will in turn heat the Kapton film. Since the thermal resistance of the thicker Kapton film has decreased, heating power that's generated by Joule heating of the Ti/Au layer is transferred more readily to the capacitor.

Since the Kapton and metal layer thicknesses were both increased, the thermal resistance of each should be examined to determine which layer has the biggest impact on thermal resistance. Figure 6.5 shows the thermal resis-

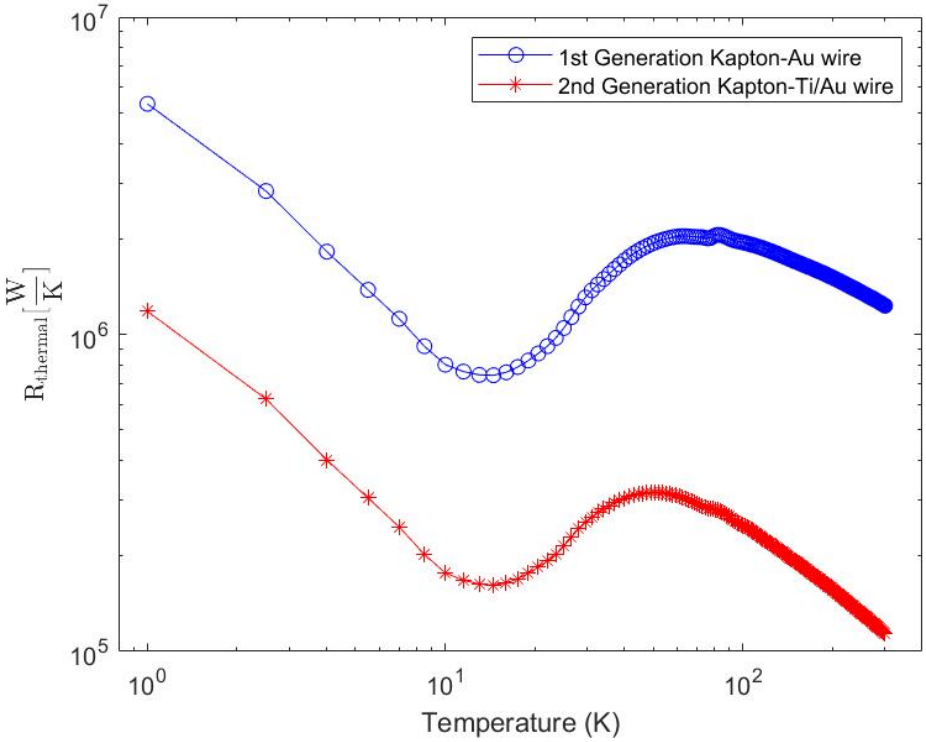


Figure 6.4: Thermal resistance of the 7$\mu$m thick Kapton-Au wires and 50$\mu$m thick Kapton-Ti/Au wires of same width and length.

tance of a 7 $\mu$m thick Kapton sheet, a 30 nm layer of Au, a 50 $\mu$m thick Kapton sheet, a 20 nm layer of Ti, and an 80 nm layer of Au, all of the same width and length. For both thicknesses of Kapton, the thermal resistance of the Kapton dominates compared with the thermal resistance of an Au or Ti/Au metal layer.

The excitation voltage of the capacitance bridge was reduced, allowing for capacitance measurements of C1 to be taken. Decreasing the excitation voltage will in turn decrease the heating power, decreasing the bandwidth of Johnson-Nyquist noise produced in the wire [39].

## 6.2 Sensitivity Considerations

With the new C1 mounted in the sample puck, the experimental apparatus was put under vacuum, and the Lake Shore temperature as well as the capacitance of each capacitor was measured and recorded at ambient lab

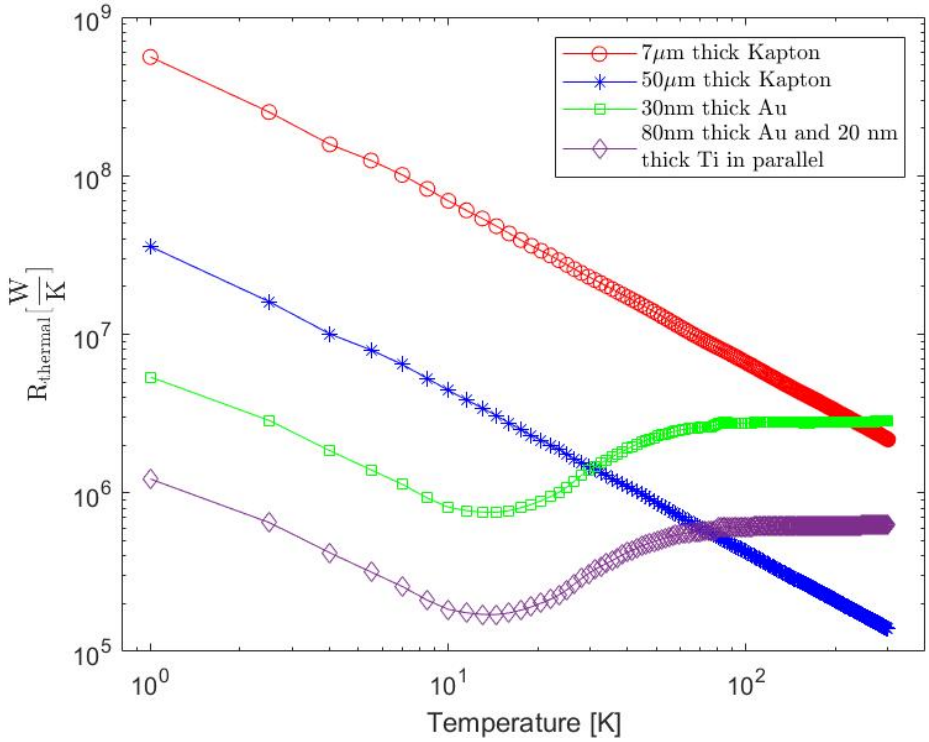


Figure 6.5: Thermal resistance of a 7$\mu$m thick Kapton film, a 50$\mu$m thick Kapton film, a 30 nm thick Au film, and a 20 nm thick Ti film added in parallel with an 80 nm thick Au film. All films have the same width and length.

temperature.

During data collection, there was a section of data where the lab temperature changed from 295.5K to 293.6K, and a section where the lab temperature was stable at ∼293.6K. As seen in figure 6.6, it can be seen that the room temperature sensitivity of the new capacitor (C1) is comparable with the $\sim 3 \times 10^{-3}$ $\frac{1}{K}$ from section 5.1.

The system was then cooled to liquid nitrogen temperatures for the next stage of preliminary testing, and the sensitivity of each thermometer was measured as seen in figure 6.7. The sensitivity of each capacitor is similar to that of figure 5.2, though it's important to note that C1 and C2 have both been re-fabricated, and the wiring of C3 has changed (see sections 4.3.2, 4.4, 5.3.1, and 6.1). The fact that the sensitivity of each thermometer in figure

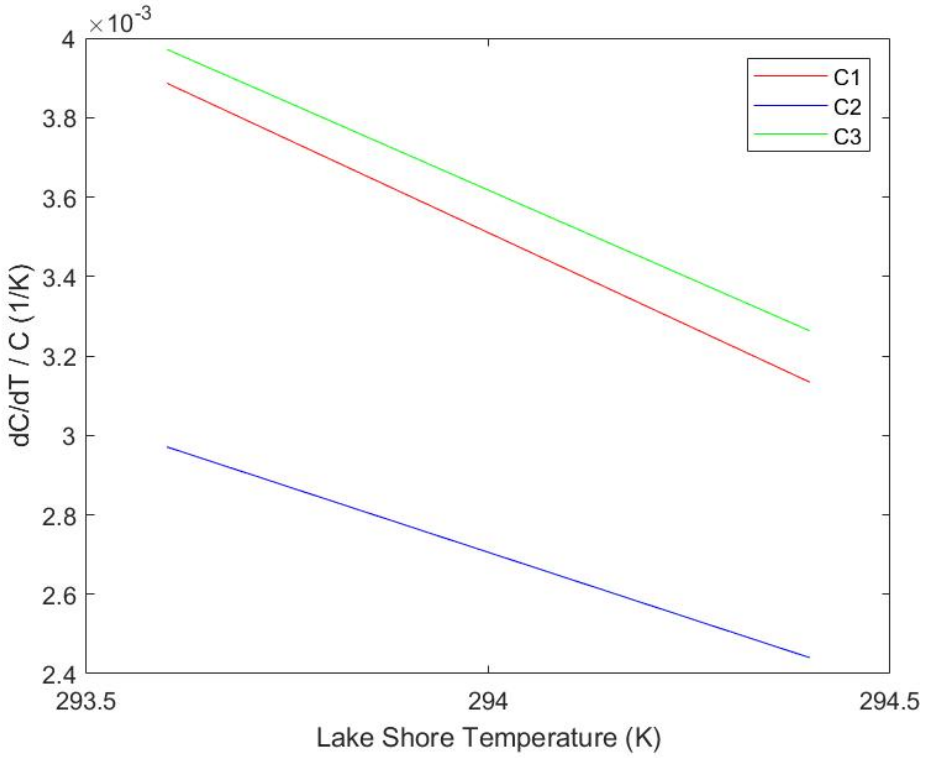


Figure 6.6: Room temperature sensitivities of the three capacitive thermometers.

6.7 is similar to that of figure 5.2 is an indication that the Ti adhesion layer on C1 is not having some adverse effect on the capacitor's function as a thermometer, and that fabrication techniques aren't drastically altering the behaviour of the capacitors.

In fact, the sensitivity has remained higher than Tinsman *et al.* [26] at each excitation voltage. As discussed in section 5.2.1, this may be due to a shift in the dielectric constant temperature dependence, shifting the temperature at which peak sensitivity occurs. Testing down to 1K, the base temperature of the cryostat, will be required to conclude the exact cause of this difference in sensitivity.

## 6.3 Noise and Resolution Considerations

Though the sensitivity is largely unchanged, measurement noise also needs to be considered when examining thermometer resolution. The standard devia-

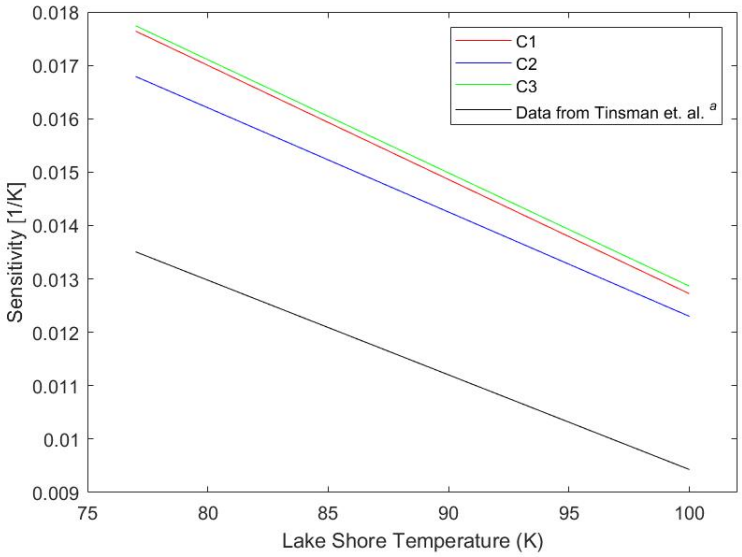


Figure 6.7: Sensitivity of each capacitor at liquid nitrogen temperatures.

[a]Data from [26]

tion of each capacitor at each excitation voltage is examined for heat off data points, as this provides insight into how much each capacitor is fluctuating about a heat off averaged capacitance value. The standard deviation of each capacitor at each excitation voltage is seen in figure 6.8. Further discussion of why the standard deviation was chosen to quantify noise for this data set is seen in appendix C.

As seen in figure 6.8, measurement noise starts to decrease with decreasing excitation voltage, as predicted by Tinsman *et al.* [26]. However, below an excitation voltage of 0.1V for C2 and C3 and of 0.005V for C1, the noise actually starts to increase with decreasing excitation voltage. This appears to be a signal-to-noise issue. As the signal sent by the capacitance bridge decreases, the inherent noise in measurements starts to dominate the measured values. As seen in table 6.2, excitation voltages lower than 0.1V are best suited for measuring capacitances anywhere from ∼100 to ∼10,000 times as large as the capacitance values currently being measured at liquid nitrogen temperatures.

At excitation voltages greater than 0.375V, measurement noise starts to increase with increasing excitation voltage. Joule heating of the wiring for each thermometer may be contributing to noise at the higher excitation volt-

Table 6.2: Capacitance bridge voltage limit for various capacitance ranges from [32]

| Voltage (V) | Max. Expected Capacitance (pF) |
|---|---|
| 15.0 | 80 |
| 7.5 | 160 |
| 3.75 | 160 |
| 3.0 | 400 |
| 1.50 | 800 |
| 0.75 | 1,600 |
| 0.375 | 1,600 |
| 0.250 | 4,800 |
| 0.125 | 4,800 |
| 0.100 | 12,000 |
| 0.050 | 12,000 |
| 0.030 | 40,000 |
| 0.015 | 40,000 |
| 0.010 | 120,000 |
| 0.0050 | 120,000 |
| 0.0030 | 400,000 |
| 0.0015 | 400,000 |
| 0.0010 | 1,200,000 |
| 0.0005 | 1,200,000 |

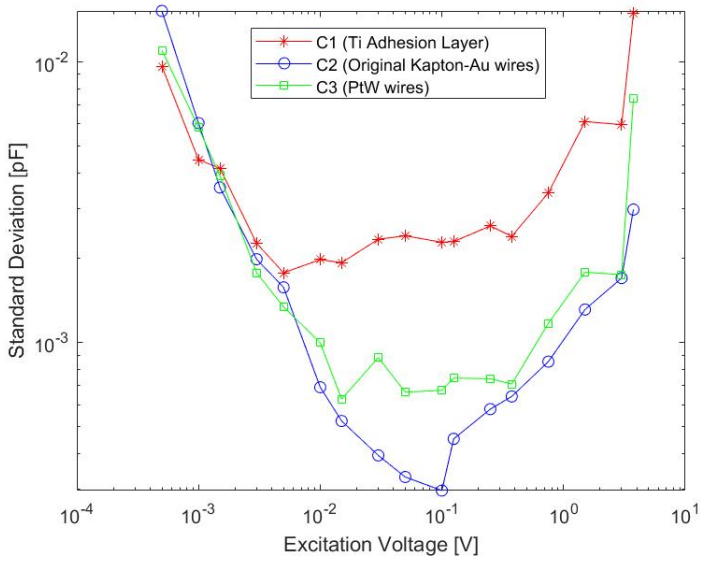


Figure 6.8: Standard deviation at ∼100K of each capacitor for every excitation voltage that the capacitance bridge can output

ages, as evidenced by the increase in standard deviation between C1 (which is wired with the thicker Kapton-Ti/Au wires) and C2/C3. However, since all three capacitors display the same behaviour of noise first decreasing with decreasing excitation voltage and then increasing with decreasing excitation voltage, there is likely some other physical phenomenon causing the increase in noise at higher excitation voltages. Further study of the behaviour of STO with changing excitation voltage is required to determine if some intrinsic property of STO is causing capacitance measurements to experience an increase in noise at the higher excitation voltages.

To quantify thermometer resolution, the standard deviation of a heat off data point at ∼100K for each thermometer is considered. The standard deviation for each capacitor shows similar behaviour at ∼80K and ∼90K, as discussed in appendix C. For C1, at worst the temperature resolution is 1 part in $10^3$ (at 3.75V) and at best is 1 part in $10^4$ (any other excitation voltage). For C2, at worst the temperature resolution is 1 part in $10^3$ (at 0.0005V) and at best is 1 part in $10^5$ (at 0.1V). For C3, at worst the temperature resolution is 1 part in $10^3$ (at 0.0005V) and at best is 1 part in $10^5$ (at 0.01V).

Recall from section 4.7 that the minimum thermometer resolution required to accurately detect a thermal Hall transverse thermal current is 1 part in

$10^4$. C1 meets this requirement at excitation voltages lower than 3.75V, and C2 and C3 have a temperature resolution that's an order of magnitude better than the required 1 part in $10^4$. It's clear that C1 consistently has a worse temperature resolution than the other two thermometers, though the mechanism behind this is not clear yet. On one hand, as described in section 6.1, the thicker Kapton-Ti/Au wires are introducing more noise than the original Kapton-Au wires described in section 4.4. On the other hand, it's possible that the Ti adhesion layer on the STO wafer is introducing some new physics that hasn't been accounted for yet. Each possibility requires further investigation

From figure 5.1, it is expected that as the temperature decreases, the sensitivity of the thermometers should increase until a peak at $\sim$40K is reached. Below $\sim$40K, the sensitivity will start to decrease again, however, so should measurement noise. This can be seen as a result of figure 4.7 — as the temperature decreases, the thermal resistance of the experimental components increases. This will result in a reduction of unwanted transfers of heating power, which will in turn decrease fluctuations of capacitance and, therefore, temperature measurements.

# Chapter 7

# Future Design Considerations and Final Comments

Overall, the experimental setup construction is nearing completion. Preliminary testing shows that the capacitive thermometers chosen for this experiment satisfy sensitivity and temperature resolution requirements outlined in section 4 to accurately perform thermal Hall measurements. The biggest hurdle to actually achieving thermal Hall measurements at this time is the fabrication of thermometers that maintain reliable adequate electronic connection upon thermal cycling.

The STO thermometer that had a titanium adhesion layer included in the fabrication process, as outlined in section 6.1, shows promise for surviving thermal cycling. The next step in testing this fabrication process is to replace the 50$\mu$m thick Kapton-Ti/Au wires on this thermometer with 7$\mu$m thick Kapton-Ti/Au wires. This will isolate whether the increased electronic noise seen in figure 6.8 originates from the thicker Kapton-Ti/Au wires, or some unknown interaction with evaporating Ti on the surface of the STO wafer.

Once it is confirmed that the STO thermometers reliably maintain electronic connection upon cooldown, the full functionality of the experimental setup may be tested. The first phase of testing will involve simply performing a longitudinal thermal conductivity measurement on the silver wire sample described in section 4.5 without a magnetic field applied, using 2 of the thermometers as longitudinal "hot" thermometers and one as a longitudinal "cold" thermometer. The results can then be compared with literature, but also since there are effectively 2 sets of thermometers performing the same experiment, the thermal conductivity measured by each set can be compared

with each other to ensure consistency.

Then, a magnetic field will be applied to the experiment. First, the expectation that the capacitive thermometers will be insensitive to magnetic fields will be verified. Then, thermal Hall measurements can be taken on a material that can be compared with literature, such as bismuth [26] or $Tb_2Ti_2O_7$ [4], [23]. Upon successfully completing the testing procedures as described above, the experiment can be used to measure materials of interest, such as proposed topological Kondo insulator candidate $SmB_6$.

# References


[1] W.H. Toews and R.W. Hill. "A robust and well shielded thermal conductivity device for low temperature measurements". In: *Review of scientific instruments* (2014).

[2] W.H Toews. "An investigation of low energy quasiparticle excitations via thermal transport measurements". PhD thesis. 2017.

[3] S. Y. Li, J.B. Bonnemaison, A. Payeur, P. Fournier, C. H. Wang, X. H. Chen, and L. Taillefer. "Low-temperature phonon thermal conductivity of single-crystalline $Nd_2CuO_4$ : Effects of sample size and surface roughness". In: *Physical review.B, Condensed matter and materials physics* 77.13 (2008). DOI: 10.1103/PhysRevB.77.134501.

[4] M. Hirschberger, J.W. Krizan, R.J. Cava, and N.P. Ong. "Large thermal Hall conductivity of neutral spin excitations in a frustrated quantum magnet". In: *Science* (2015).

[5] G. Grissonnanche, S. Thériault, A. Gourgout, M.E. Boulanger, E. Lefrançois, A. Ataei, F. Laliberté, M. Dion, J.S. Zhou, S. Pyon, T. Takayama, H. Takagi, N. Doiron-Leyraud, and L. Taillefer. "Chiral phonons in the pseudogap phase of cuprates". In: *Nature physics* (2020).

[6] G. Grissonnanche, A. Legros, S. Badoux, E. Lefrançois, V. Zatko, M. Lizaire, F. Laliberté, A. Gourgout, J.S. Zhou, S. Pyon, T. Takayama, H. Takagi, S. Ono, N. Doiron-Leyraud, and L. Taillefer. "Giant thermal Hall conductivity in the pseudogap phase of cuprate superconductors". In: *Nature* (2019).

[7] T. Yokoi, S. Ma, Y. Kasahara, S. Kasahara, T. Shibauchi, N. Kurita, H. Tanaka, J. Nasu, Y. Motome, C. Hickey, S. Trebst, and Y. Matsuda. "Half-integer quantized anomalous thermal Hall effect in the Kitaev material candidate $\alpha$-$RuCl_3$". In: *Science* (2021).

[8] Y. Kasahara, T. Ohnishi, Y. Mizukami, O. Tanaka, S. Ma, K. Sugii, N. Kurita, H. Tanaka, J. Nasu, Y. Motome, T. Shibauchi, and Y. Matsuda. "Majorana quantization and half-integer thermal quantum Hall effect in a Kitaev spin liquid". In: *Nature (London); Nature* 559.7713 (2018), pp. 227–231. DOI: 10.1038/s41586-018-0274-0.

[9] M. Dzero, J. Xia, V. Galitski, and P. Coleman. "Topological Kondo Insulators". In: *Annual review of condensed matter physics* 7.1 (2016), pp. 249–280. DOI: 10.1146/annurev-conmatphys-031214-014749.

[10] M. Franz and L. Molenkamp. *Topological insulators*. Amsterdam: Elsevier Science, 2013. ISBN: 9780444633149.

[11] P. Coleman. *Introduction to many-body physics*. Cambridge, United Kingdom: Cambridge University Press, 2015. ISBN: 9780521864886.

[12] L. Fu and C.L. Kane. "Topological insulators with inversion symmetry". In: *Physical review B, Condensed matter and materials physics* 76.4 (2007). DOI: 10.1103/PhysRevB.76.045302.

[13] Marcel Franz and Laurens Molenkamp. *Topological insulators*. Amsterdam: Elsevier Science, 2013. ISBN: 9780444633149.

[14] L. Kouwenhoven and L. Glazman. "Revival of the Kondo effect". In: *Physics world* 14.1 (2001), pp. 33–38. DOI: 10.1088/2058-7058/14/1/28.

[15] P. Coleman. "Condensed matter: strongly correlated electrons". In: *Physics world* 8.12 (1995), pp. 29–36. DOI: 10.1088/2058-7058/8/12/20.

[16] M. Dzero, K. Sun, V. Galitski, and P. Coleman. "Topological Kondo insulators". In: *Physical Review Letters; Phys Rev Lett* 104.10 (2010), pp. 106408–106408. DOI: 10.1103/PhysRevLett.104.106408.

[17] D.J. Kim, T. Grant, and Z. Fisk. "Limit cycle and anomalous capacitance in the Kondo insulator $SmB_6$". In: *Physical Review Letters; Phys Rev Lett* 109.9 (2012). DOI: 10.1103/PhysRevLett.109.096601.

[18] X. Zhang, N.P. Butch, P. Syers, S. Ziemak, R.L. Greene, and J. Paglione. "Hybridization, Inter-Ion Correlation, and Surface States in the Kondo Insulator $SmB_6$". In: *Physical review X* 3.1 (2013). DOI: 10.1103/PhysRevX.3.011011.

[19] S. Wolgast, Ç. Kurdak, K. Sun, J.W. Allen, D.J. Kim, and Z. Fisk. "Low-temperature surface conduction in the Kondo insulator $SmB_6$". In: *Physical review B, Condensed matter and materials physics* 88.18 (2013). DOI: 10.1103/PhysRevB.88.180405.

[20] D.J. Kim, S. Thomas, T. Grant, J. Botimer, Z. Fisk, and J. Xia. "Surface hall effect and nonlocal transport in $SmB_6$: evidence for surface conduction". In: *Scientific reports; Sci Rep* 3.1 (2013), pp. 3150–3150. DOI: 10.1038/srep03150.

[21] L. Li, K. Sun, C. Kurdak, and J.W. Allen. "Emergent mystery in the Kondo insulator samarium hexaboride". In: *Nature Reviews Physics* 2.9 (2020), pp. 463–479. DOI: doi.org/10.1038/s42254-020-0210-8.

[22] M.G. Holland and L.G. Rubin. "Apparatus for the Measurement of Thermal Conductivity in the Range 1.7 to 300°K". In: *Review of scientific instruments* 33.9 (1962), pp. 923–928. DOI: 10.1063/1.1718028.

[23] H.L. Kim, M.J. Coak, J.C. Baglo, K. Murphy, R.W. Hill, M. Sutherland, M.C. Hatnean, G. B., and J.G. Park. "Modular thermal Hall effect measurement setup for fast-turnaround screening of materials over wide temperature range using capacitive thermometry". In: *Review of scientific instruments* 90.10 (2019), p. 103904. DOI: 10.1063/1.5108512.

[24] D.R. Smith and F.R. Fickett. "Low-temperature properties of silver". In: *Journal of research of the National Institute of Standards and Technology; J Res Natl Inst Stand Technol* 100.2 (1995), pp. 119–171. DOI: 10.6028/jres.100.012.

[25] D.R. White, R. Galleano, A. Actis, H. Brixy, M.D. Groot, J. Dubbeldam, A.L. Reesink, F. Edler, H. Sakurai, R.L. Shepard, and J.C. Gallop. "The status of Johnson noise thermometry". In: *Metrologia* 33.4 (1996), pp. 325–335. DOI: 10.1088/0026-1394/33/4/6.

[26] C. Tinsman, G. Li, C. Su, T. Asaba, B. Lawson, F. Yu, and L. Li. "Probing the thermal Hall effect using miniature capacitive strontium titanate thermometry". In: *Applied Physics Letters* 108.26 (2016), p. 261905. DOI: 10.1063/1.4955069.

[27] H.E. Weaver. "Dielectric properties of single crystals of $SrTiO_3$ at low temperatures". In: *The Journal of physics and chemistry of solids* 11.3 (1959), 274, IN5, 275–274, IN6, 277. DOI: 10.1016/0022-3697(59)90226-4.

[28] M. J. Coak. "Quantum Tuning and Emergent Phases in Charge and Spin Ordered Materia". PhD thesis. 2017.

[29] M.C. Runyan and W.C. Jones. "Thermal conductivity of thermally-isolating polymeric and composite structural support materials between 0.3 and 4 K". In: *Cryogenics (Guildford)* 48.9 (2008), pp. 448–454. DOI: 10.1016/j.cryogenics.2008.06.002.

[30] G.K. White. “The Thermal Conductivity of Gold at Low Temperatures”. In: *Proceedings of the Physical Society, Section A* 66.6 (1953), pp. 559–564. DOI: 10.1088/0370-1298/66/6/307.

[31] J.R. Rumble. “CRC Handbook of Chemistry and Physics”. In: 103rd Edition (Internet Version 2022). Boca Raton, FL: CRC Press/Taylor Francis, 2022.

[32] Andeen-Hagerling. *AH 2500A 1kHz Ultra-Precision Capacitance Bridge Operation and Maintenance Manual*. Cleveland, OH, USA, 1994.

[33] J.E. Tuttle, E. Canavan, and M. DiPirro. “Thermal and Electrical Conductivity Measurements of CDA 510 Phosphor Bronze”. In: vol. 1219. 2010. Chap. AIP Conference Proceedings, p. 55.

[34] H. Hieber. “Aging properties of gold layers with different adhesion layers”. In: *Thin Solid Films* 37.3 (1976), pp. 335–343. DOI: 10.1016/0040-6090(76)90603-9.

[35] M. Todeschini, F. Jensen A.B.d.S. Fanta, J.B.l Wagner, and A. Han. “Influence of Ti and Cr Adhesion Layers on Ultrathin Au Films”. In: *ACS applied materials & interfaces* 9.42 (2017), pp. 37374–37385. DOI: 10.1021/acsami.7b10136.

[36] K. W. Vogt, P. A. Kohl, W. B. Carter, R. A. Bell, and L. A. Bottomley. “Characterization of thin titanium oxide adhesion layers on gold: resistivity, morphology, and composition”. In: *Surface Science* 301.1 (1994), pp. 203–213. DOI: 10.1016/0039-6028(94)91300-5.

[37] Y. Peysson, C. Ayache, B. Salce, S. Kunii, and T. Kasuya. “Thermal conductivity of CeB6 and LaB6”. In: *Journal of Magnetism and Magnetic Materials* 59.1-2 (1986), pp. 33–40. DOI: 10.1016/0304-8853(86)90007-7.

[38] K. Flachbart, M. Reiffers, S. Molokác, A. Belling, J. Bischof, E. Konovalova, and Y. Paderno. “Thermal conductivity of LaB6: the role of phonons”. In: *Physica.B, Condensed matter* 263-264 (1999), pp. 749–751. DOI: 10.1016/S0921-4526(98)01456-2.

[39] J.B. Johnson. “Thermal agitation of electricity in conductors”. In: *Physical review* 32.1 (1928), pp. 97–109. DOI: 10.1103/PhysRev.32.97.

[40] A.L. Woodcraft and A. Gray. “A low temperature thermal conductivity database”. In: *13th International Low Temperature Detectors Workshop*. Vol. 1185. American Institute of Physics, 2009, pp. 681–684. ISBN: 0094-243X. DOI: 10.1063/1.3292433.

[41] D. J. Benford, T. J. Powers, and S. H. Moseley. "Thermal conductivity of Kapton tape". In: *Cryogenics (Guildford)* 39.1 (1999), pp. 93–95.

[42] M. Barucci, E. Gottardi, I. Peroni, and G. Ventura. "Low temperature thermal conductivity of Kapton and Upilex". In: *Cryogenics (Guildford)* 40.2 (2000), pp. 145–147.

[43] W. Kobayashi, Y. Koizumi, and Y. Moritomo. "Large thermal Hall coefficient in bismuth". In: *Applied Physics Letters* 100.1 (2012), pp. 011903-011903–3. DOI: 10.1063/1.3673562.

[44] M.E. Boulanger, G. Grissonnanche, S. Badoux, A. Allaire, É. Lefrançois, A. Legros, A. Gourgout, M. Dion, C.H. Wang, X.H. Chen, R. Liang, W.N. Hardy, D.A. Bonn, and L. Taillefer. "Thermal Hall conductivity in the cuprate Mott insulators Nd2CuO4 and Sr2CuO2Cl2". In: *Nature communications* 11.1 (2020), pp. 5325–5325. DOI: 10.1038/s41467-020-18881-z.

[45] R.L. Rosenbaum. "Some Properties of Gold-Iron Thermocouple Wire". In: *Review of scientific instruments* 39.6 (1968), pp. 890–899. DOI: 10.1063/1.1683532.

[46] A. V. Inyushkin, K. Leicht, and P. Esquinazi. "Magnetic field dependence of the sensitivity of a type E (chromel–constantan) thermocouple". In: *Cryogenics (Guildford)* 38.3 (1998), pp. 299–304. DOI: 10.1016/S0011-2275(97)00156-2.

[47] C. Strohm, G. L. J. A. Rikken, and P. Wyder. "Phenomenological evidence for the phonon hall effect". In: *Physical Review Letters; Phys Rev Lett* 95.15 (2005), pp. 155901–155901. DOI: 10.1103/PhysRevLett.95.155901.

[48] M. Affronte, M. Campani, B. Morten, M. Prudenziati, and O. Laborde. "Magnetoresistance of RuO2-Based Thick Film Resistors". In: *Journal of Low Temperature Physics* 112.5-6 (1998), pp. 355–371. DOI: 10.1023/a:1022336702261.

[49] *Lake Shore Cryotronics*. https://www.lakeshore.com/products/categories/specification/temperature-products/cryogenic-temperature-sensors/cernox. Accessed: 2022-10-13.

# Appendices

# Appendix A

# Thermal conductivities of experimental components

Thermal conductivity values from figure A.1 are used for all calculations of thermal resistance in this work. The source of each set of data is listed in the figure caption.

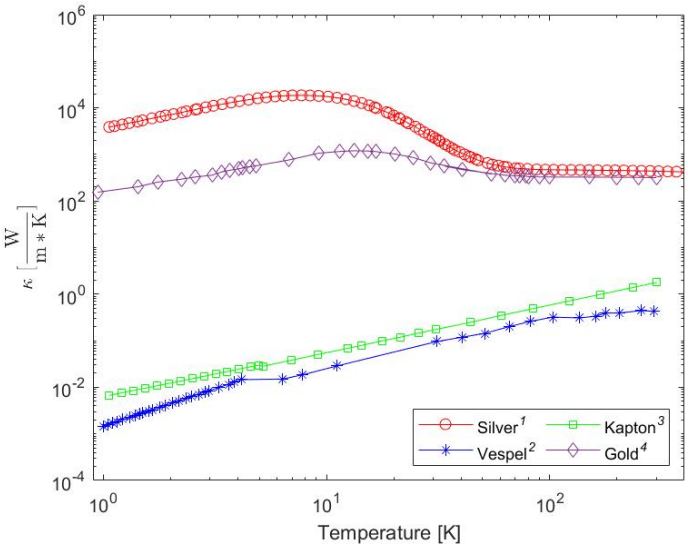


Figure A.1: Thermal conductivity of each experimental component.

[1]Data from [31] and [24]
[2]Data from [40] and [29]. Note that above 4K, thermal conductivity data for vespel SP-22 (used in this work) is unavailable, and instead data for vespel SP-1 is used
[3]Data from [41] and [42]
[4]Data from [31] [30]
[5] Data from [31]

# Appendix B

# Kapton-Ag and PtW Noise Comparison

Preliminary testing of Kapton wiring was completed before the construction of the experiment from this work was started. Due to the significant cost difference between silver and gold, silver was chosen as the metal to evaporate onto Kapton sheets as described in section 4.4.

Testing was completed on the research group's existing thermal conductivity sample boxes described in [1]. One resistive thermometer's wiring was swapped from PtW coils to the newly fabricated Kapton-Ag wires, while the other resistive thermometer's wiring was kept as PtW coils.

Instead of using the experimental process as outlined in section 4.6, the sample box was cooled to liquid nitrogen base temperature, and the resistance of each thermometer along with the Lake Shore resistance and temperature were recorded as the system sat at ∼77K.

This however means that the temperature was allowed to drift as ambient lab conditions varied. This temperature drift can be seen in figure B.1. The temperature decreased approximately linearly from ∼77.32 K to ∼77.30 K over the span of data collection. A background linear fit was subtracted from each data set to produce figure 5.6. Note also that the resolution of the resistance measurements is 0.01Ω, so it's possible that noise experienced during these measurements may be smaller than changes in resistance that the resistance bridge can resolve.

When construction of the experimental setup described in this work began, the Kapton-Ag wires were scrapped in favour of Kapton-Au wires. The

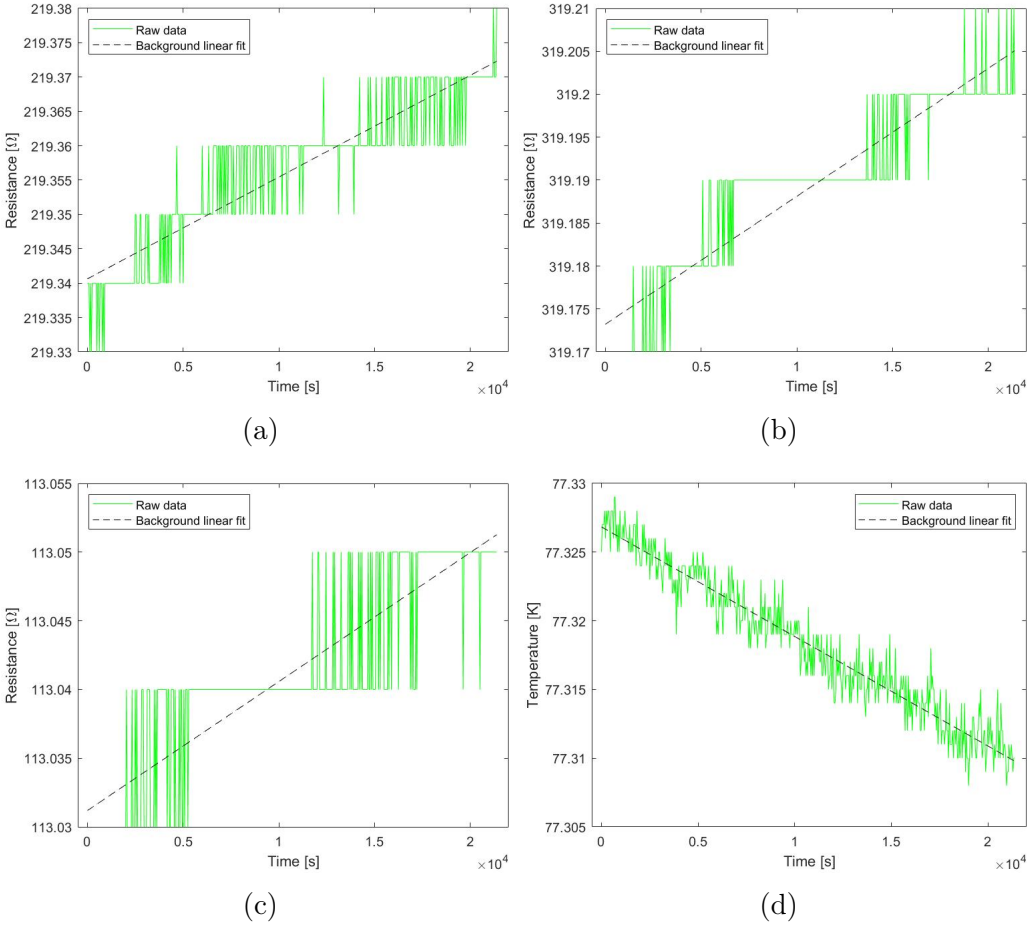


Figure B.1: Raw data used to calculate residuals for figure 5.5, for (a) sample resistive thermometer 1 resistance over time, (b) sample resistive thermometer 2 resistance over time, (c) Lake Shore temperature controller resistive thermometer resistance over time, and (d) Lake Shore temperature controller resistive thermometer — resistance values converted to temperature values over time. Note the background linear temperature drift over time — this is subtracted from the data set, and the residuals for each thermometer are calculated from the background-subtracted data.

Kapton-Ag wires were fabricated prior to university closures caused by the COVID-19 pandemic, and the sample puck as described in chapter 4 began approximately 2 years later. In that time, the Kapton-Ag wires had started to oxidize, so it was decided that since preliminary testing on the Kapton-Ag showed a reduction in noise (see section 5.3.1), Kapton-Au wires would be used for this work.

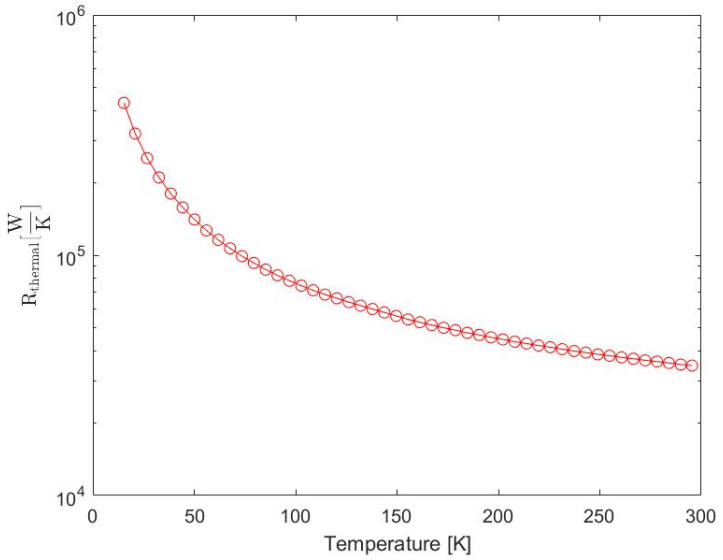


Figure B.2: Thermal resistance estimate of PtW coils from [23]

As seen in figure A.1, the thermal conductivity of gold is less than that of silver. Therefore, for the same metal layer thickness and wire dimensions, a Kapton-Au wire will have a higher thermal resistance than a Kapton-Ag wire. This means that external heat transfers to the thermometer will be decreased using Kapton-Au compared with Kapton-Ag wires. So, while there is no Kapton-Au data from 2019 to compare data from this work to, the Kapton-Ag data provides a baseline of the behaviour that can be expected if Kapton-Au wires are functioning as expected.

## B.1 PtW Thermal Resistance

Figure B.2 shows the thermal resistance of PtW coils as calculated by [23]. It can then be seen from figure 4.7 that the thermal resistance of PtW coils is $\sim$2 orders of magnitude smaller than that of Kapton-Au wires.

# Appendix C

# Supplementary Data From Figure 6.8

As discussed in section 6.3, the standard deviation of each capacitor at each excitation voltage at ∼100K was calculated to quantify noise and thermometer resolution. This is a different strategy than was used in chapter 5, where fluctuations about an average value during a heat-off step was used in noise analyses. The standard deviation method was chosen for section 6.3 due to logistical reasons — namely, it was infeasible to effectively display noise data for each capacitor at each excitation voltage.

Standard deviation is a measure of a data set's dispersion. In other words, standard deviation can be used to quantify fluctuations about a data set's average value. However, this is only true if there is no time dependent drift in the average value, which may be caused by factors such as thermometer self-heating, or temperature controller settings. As seen in figure C.1, there is no time dependent drift in the temperature as measured by the Lake Shore temperature controller, so the standard deviation data displayed in figure 6.8 is a measure of fluctuations about the average.

As seen in figure C.2, the standard deviation of each capacitor at each excitation voltage at ∼80K and ∼90K shows similar behaviour as the ∼100K data displayed in figure 6.8. This means that the resolution of each thermometer as outlined in section 6.3 is the same at ∼80K and ∼90K.

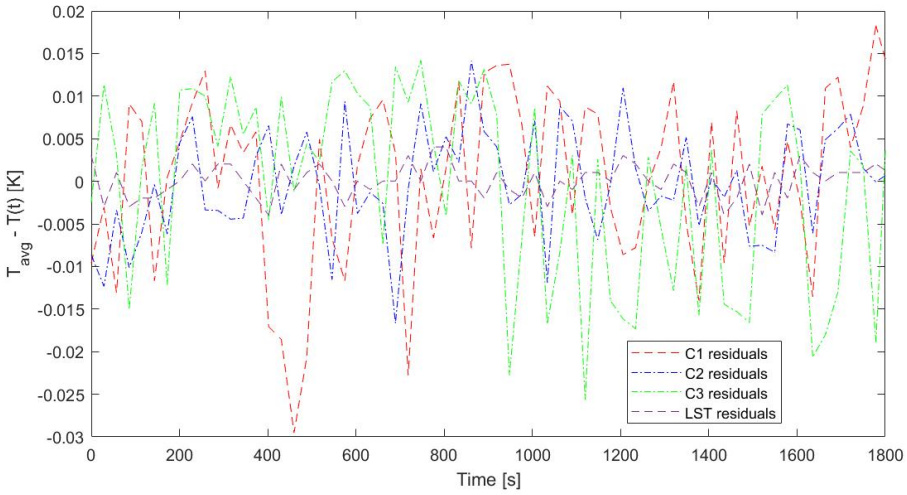


(a) 3.75V excitation voltage

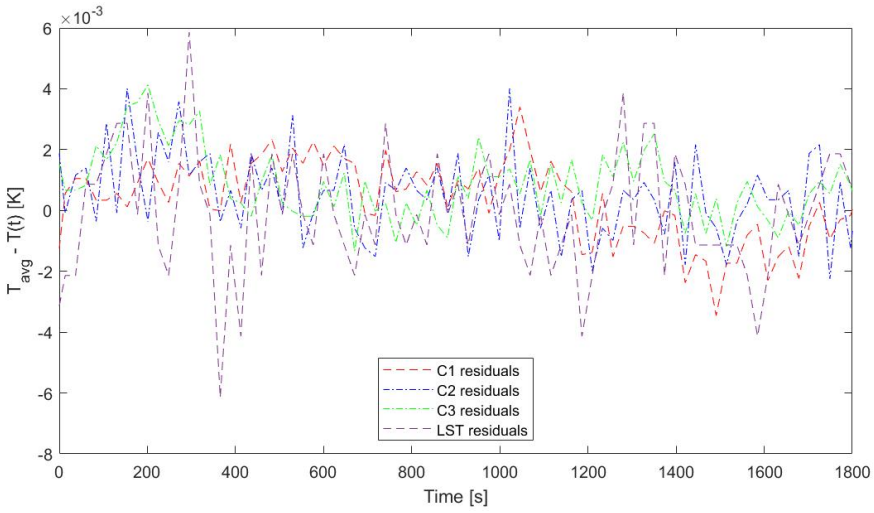


(b) 0.01V excitation voltage

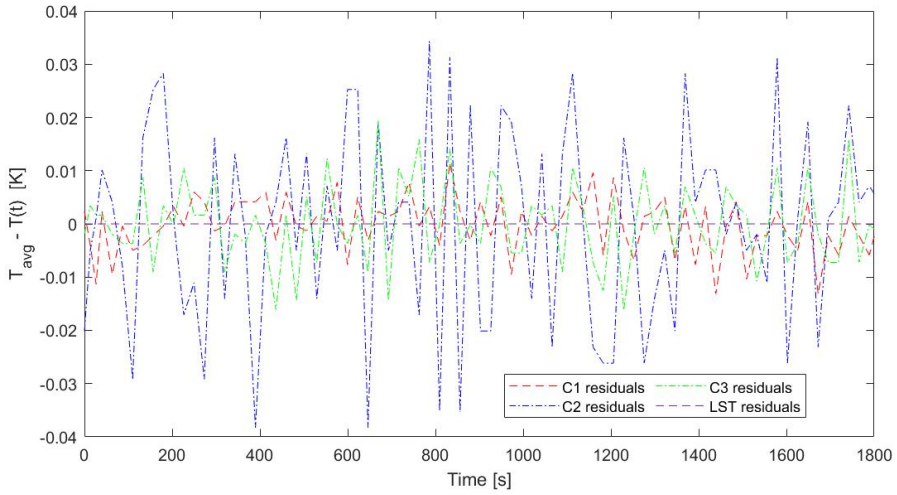


(c) 0.001V excitation voltage

Figure C.1: Temperature residuals for each capacitive thermometer and the Lake Shore thermometer over a 100K heat-off averaging step, at three capacitance bridge excitation voltages. Residuals are calculated as the difference between the average temperature and the real-time temperature.

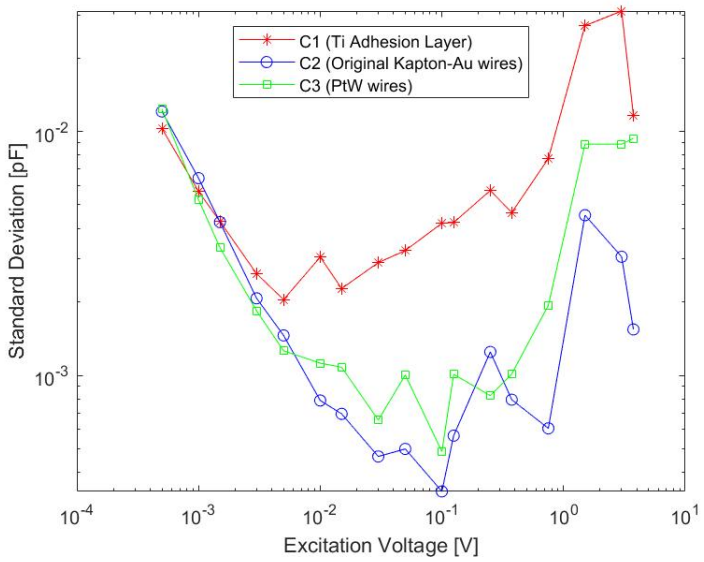


(a) ∼80K data

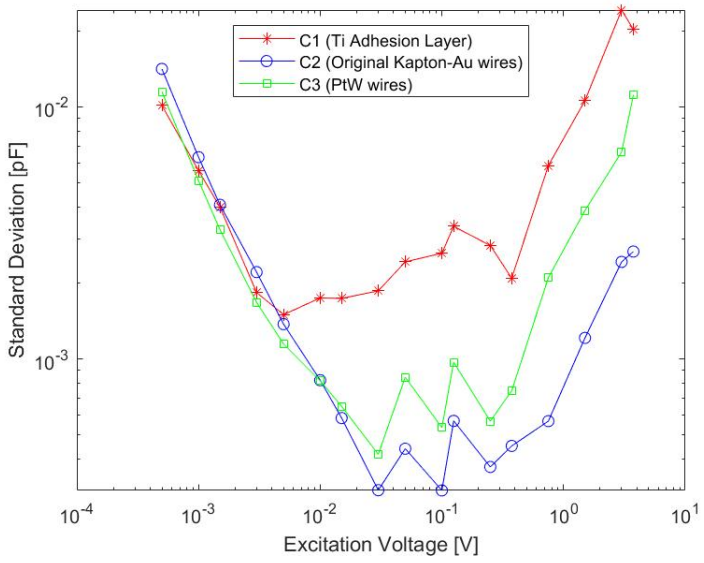


(b) ∼90K data

Figure C.2: Standard deviation at ∼80K and ∼90K of each capacitor for every excitation voltage that the capacitance bridge can output

# Appendix D

# Review of Commonly Used Thermometers for Thermal Hall Experiments

## D.1 Thermocouples

Thermocouples can be used to measure the sample temperature gradient in the longitudinal and transverse directions [43], [44], [5]. Thermocouples are fabricated by joining two dissimilar metallic wires. When the temperature of the junction of those two wires changes, a voltage is generated across the junction. Therefore, a change in measured voltage of the junction can be a probe of the change in temperature.

Kobayashi *et al.* [43] used Au(Fe 0.07%)-chromel thermocouples. The benefit of this type of thermocouple is that it has a high sensitivity at intermediate temperatures — at 85K, these thermocouples can detect changes in temperature of 1 part in $10^4$ [45]. However, the resolution of these thermocouples decreases with decreasing temperature. At 0.4K, the thermocouples can detect temperature changes of 1 part in $10^2$ [45]. Kobayashi *et al.* [43] perform their thermal Hall measurements from 75K to room temperature, so these thermocouples are work well for their applications. However, the sensitivity at low temperatures is not appropriate for low temperature thermal Hall measurements.

Boulanger *et al.* [44] and Grissonnanche *et al.* [5] both use Type-E thermocouples, which are readily available commercially. These thermocouples have a temperature resolution of 1 part in $10^4$ at $\sim$10K, increasing to 1 part

in $10^5$ ∼100K [4]. However, they are also sensitive to magnetic fields — meaning, if the temperature of the system is held constant and a magnetic field is applied, the voltage of the thermocouples will change. This complex magnetic field dependence can be seen in figure D.1. While these thermocouples can be used for thermal Hall measurements, additional calibration of the thermocouples in field would be necessary.

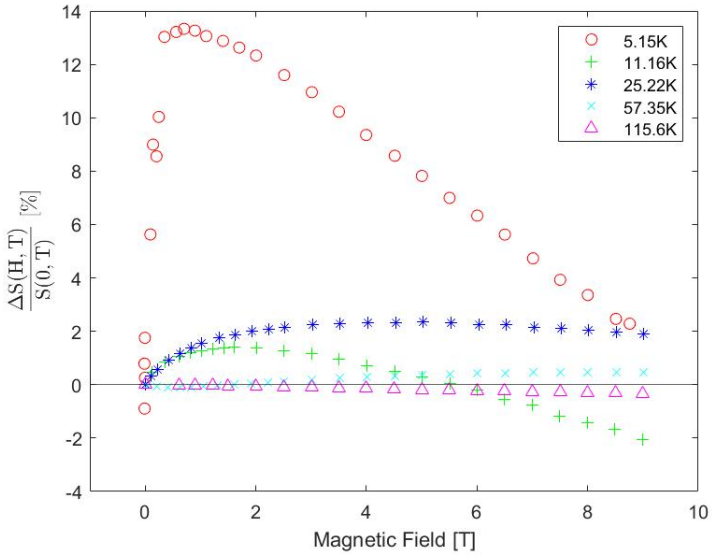


Figure D.1: Type-E thermocouple change in thermopower ($\Delta S$) with changing magnetic field from [46]

## D.2 Resistive Thermometers

Resistors with a favourable resistance temperature dependence can be used as thermometers [4], [8], [47], [1]. Ruthenium oxide resistive thermometers are commonly used at low temperatures because of their sensitivity, and Cernox resistive thermometers are commonly used at temperatures above 2K [1].

Ruthenium oxide thermometers have a temperature resolution of 1 part in $10^3$ at ∼1K [4], and Cernox resistive thermometers have a temperature resolution of 1 part in $10^4$ at ∼15K. Both thermometers are readily available commercially, however they both experience magnetoresistance in the presence of a magnetic field (ie., at a constant temperature, if the magnetic field is changed the resistance of the thermometers will change too). Figures D.2

and D.3 show the change in measured temperature with changing magnetic fields. Like Type-E thermocouples, this magnetoresistance can be compensated for by calibrating the thermometers in field.

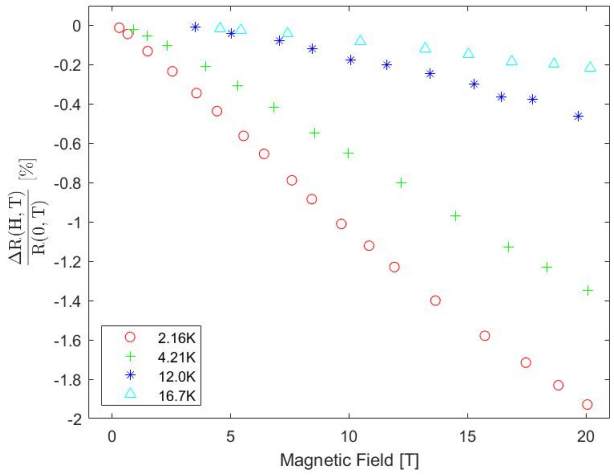


Figure D.2: $RuO_2$ change in resistance with changing magnetic field from [48]

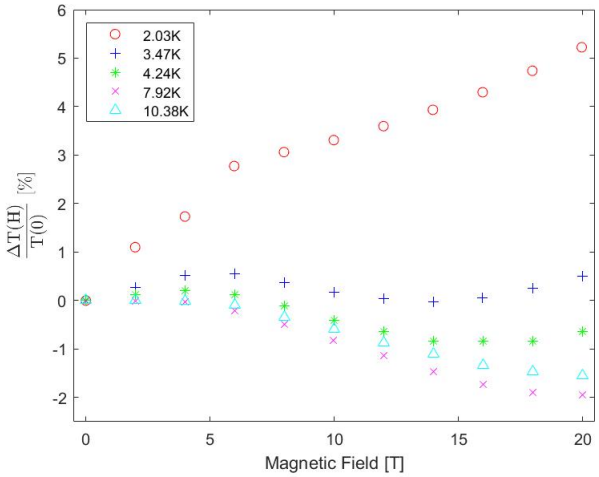


Figure D.3: Cernox resistive thermometer change in measured temperature with changing magnetic field from [49]